Ocean Modelling 117 (2017) 12–27

Contents lists available at ScienceDirect

Ocean Modelling

journal homepage: www.elsevier.com/locate/ocemod

Anomalous circulation in the Pacific sector of the Arctic Ocean in July–December 2008

Oceana P. Francis[a,*], Max Yaremchuk[b], Gleb G. Panteleev[c,1], Jinlun Zhang[d], Mikhail Kulakov[e]

[a] Department of Civil and Environmental Engineering, University of Hawai'i, HI, USA
[b] Naval Research Laboratory, Stennis Space Center, 1009 Balch Blvd., MS, USA
[c] International Arctic Research Center, University of Alaska, Fairbanks, AK, USA
[d] Applied Physics Laboratory, University of Washington, WA, USA
[e] Arctic and Antarctic Research Institute, St. Petersburg, Russia

ARTICLE INFO

Article history:
Received 27 September 2016
Revised 12 May 2017
Accepted 18 June 2017
Available online 20 June 2017

Keywords:
Arctic ocean circulation
Numerical modeling
4Dvar data assimilation

ABSTRACT

Variability of the mean summer-fall ocean state in the Pacific Sector of the Arctic Ocean (PSAO) is studied using a dynamically constrained synthesis (4Dvar) of historical in situ observations collected during 1972 to 2008. Specifically, the oceanic response to the cyclonic (1989–1996) and anticyclonic (1972–1978, 1997–2006) phases of the Arctic Ocean Oscillation (AOO) is assessed for the purpose of quantitatively comparing the 2008 circulation pattern that followed the 2007 ice cover minimum.

It is shown that the PSAO circulation during July-December of 2008 was characterized by a pronounced negative Sea Surface Height (SSH) anomaly along the Eurasian shelf break, which caused a significant decline of the transport in the Atlantic Water (AW) inflow region into the PSAO and increased the sea level difference between the Bering and Chukchi Seas. This anomaly could be one of the reasons for the observed amplification of the Bering Strait transport carrying fresh Pacific Waters into the PSAO. Largrangian analysis of the optimized solution suggests that the freshwater (FW) accumulation in the Beaufort Gyre has a negligible contribution from the East Siberian Sea and is likely caused by the enhanced FW export from the region north of the Canadian Archipelago/Greenland.

The inverse modeling results are confirmed by validation against independent altimetry observations and in situ velocity data from NABOS moorings. It is also shown that presented results are in significantly better agreement with the data than the output of the PIOMAS model run utilized as a first guess solution for the 4dVar analysis.

1. Introduction

In recent years, studies of the Arctic Ocean circulation and the freshwater (FW) budget have gained considerable attention due to its influence on the global climate system. Ice conditions and the circulation in the Arctic Ocean have undergone a particularly pronounced change, including a persistent decrease in ice cover at an average rate of 15% per decade (IPCC, 2013) accompanied by the tremendous ice retreats of 2007 and 2012, when most of the Pacific Sector of the Arctic Ocean (PSAO) became almost completely ice-free in the summer (Zhang et al., 2013). These processes are well correlated with other observed phenomena such as: enhanced wind-driven vertical mixing during the ice free periods (e.g. Yang et al., 2004; Kawagachi, 2015), a tendency for intensification of the flow through the Bering Strait during 2007–2009 (Woodgate et al., 2010), and an increase in significant wave height (Francis et al., 2011). During the summer, increased storm activity may cause an additional reduction of the ice cover due to storm-generated mixing in the upper ocean (Zhang et al., 2013; Long and Perrie, 2012). The enhanced wave-ice interaction in the marginal ice zones and wave induced mixing also contributes towards the decrease of ice (Williams et al., 2013a; 2013b; Qiao et al., 2004). These processes may significantly accelerate the observed changes in the ice conditions and affect accumulation and redistribution of the freshwater in the Arctic Ocean (e.g. Woodgate et al., 2012).

The outflow of low-salinity Arctic Water into the North Atlantic, one of the most important advective sources of liquid freshwater

* Corresponding author at: Department of Civil and Environmental Engineering, University of Hawai'i at Mānoa, 2540 Dole Street, Holmes Hall 383, Honolulu, HI 96822, USA
E-mail address: oceanaf@hawaii.edu (O.P. Francis).
[1] Now in Naval Research Laboratory, Stennis Space Center, 1009 Balch Blvd., MS,, USA

http://dx.doi.org/10.1016/j.ocemod.2017.06.006
1463-5003/

in the World Ocean, is crucial for maintaining the global conveyer belt forced by the Atlantic Meridional Overturning Circulation (e.g. Jones and Anderson, 2008).

Alternatively, redistribution of the salty Atlantic, relatively fresh Pacific water, and riverine water within the Arctic Ocean are the key factors controlling thermohaline circulation and FW distribution within the Arctic Ocean (e.g., Jones et al., 1998). Importantly, the FW deficit in the surface layers may cause fast erosion of the pycnocline and enhanced vertical mixing. This may bring relatively warm Atlantic water (AW) to the surface and accelerate the observed trend of the diminishing ice cover in the Arctic Ocean (e.g. Carmack et al., 2015). Because of the importance of the FW budget, monitoring the FW balance and redistribution has become one of the primary objectives of several large observational programs (e.g. Beaufort Gyre Exploration Program (BGEP www.whoi.edu/beaufortgyre), Nansen Amundsen Basins Observing System (NABOS http://research.iarc.uaf.edu/NABOS/), Canadian Basin Observational System (CABOS)).

In the Arctic, the FW is mostly stored within the Beaufort Gyre (BG) (Aagaard and Carmack, 1989). According to Proshutinsky et al. (2002), wind is the major forcing responsible for the accumulation of FW in the Beaufort Sea through the convergence in the Ekman layer and subsequent FW downwelling in the central part of the Gyre. Intensification of this process is correlated with the Arctic Ocean Oscillation (AOO) index quantifying the Sea Surface Height (SSH) anomaly associated with the BG (Proshutinsky and Johnson, 1997). Thus, being closely connected to the regional changes in the atmospheric circulation, this relationship potentially allows large scale analysis of the FW accumulation and its export from the Arctic Ocean.

Analysis of the long-term SSH variability in the Arctic Ocean has shown that this process of FW accumulation and release is usually governed by a 5–7 year cycle (Proshutinsky et al., 2009). During cyclonic epochs (1953–1958, 1963–1970, 1980–1986, 1990–1996), the Arctic atmosphere was relatively warm and humid, while the FW outflow into the Atlantic was intensified (Proshutinsky et al., 2002; 2015). In contrast, the anticyclonic periods were characterized by the clockwise shifts in the PSAO circulation accompanied by a significant reduction in the FW export. According to this concept, the period of the positive AOO which started in 1997 should have changed sign around 2004–2006. However, the positive AOO values still persists through the years of 2005–2017. One of the hypotheses, explaining such anomalous behavior, is related to the additional FW export from Greenland which may significantly increase the periods of the positive AOO index due to the intensification of the FW advection from Greenland into the Arctic Ocean (Proshutinsky et al., 2015). It is noteworthy to mention that recent observations of FW anomalies in the Lincoln Sea (De Steur et al., 2013) appear to support this hypothesis.

Persistence of the positive AOO phase after 2007, associated with the FW accumulation and intensification of the BG was confirmed by McPhee et al. (2009) through analysis of in situ temperature and salinity observations and by Kwok and Morrison (2011) who analyzed ICEsat altimetry and diagnosed a distinct SSH dome of approximately 40 cm over the Beaufort Sea during 2004–2008. Recently, the BG intensification was also identified in a numerical study with simplified ice data assimilation by Zhang et al. (2016) who obtained a persistent amplification of the BG since 1992 and its stabilization after 2008. Analysis of a more advanced data assimilative solution (2002–2008) from the Global Ocean Reanalysis and Simulations (GLORYS1) run also revealed FW accumulation in the BG accompanied by salinization of the Eurasian Basin (Ligue et al., 2011). The authors linked these processes to specific atmospheric conditions during 2007 and 2008 and spatial re-distribution of the liquid freshwater in the Arctic Ocean. Lique et al. (2011) also diagnosed an enhanced inflow of the AW through the Fram Strait, which may lead to the observed salinization in the GLORYS1 solution. However, it is necessary to note that the above mentioned data assimilation solutions did not assimilate any oceanic and (in the case of GLORYS1) ice observations. In particular, salinization in the Eurasian Basin was not conclusively supported by McPhee et al. (2009) and Rabe et al. (2011) who analyzed the in situ observations in the Arctic Ocean.

In controversy to the above mentioned hypothesis, Morison et al. (2012) suggested that the observed BG freshening is caused by the increased sea ice melting and changes of the pathways of the Eurasian river runoff. According to this hypothesis, changes of the riverine water pathways are due to the strengthening of the eastward atmospheric circulation in the Northern Hemisphere, associated with the increased Arctic Oscillation index.

Due to a scarcity of hydrographic observations in the Arctic Ocean, most of the above mentioned in situ data analyses were performed via simple optimal interpolation by combining observations from different seasons (e.g. Proshutinsky et al., 2009; McPhee et al., 2009). To analyze interannual variability, it is also necessary to specify background fields in the regions where the observations were absent for a particular year (e.g. Proshutinsky et al., 2009). Taking the background from previous years may lead to significant errors in the derived temperature-salinity distributions due to the homogeneity of the correlation functions (MacIntosh, 1990) and time variations of the background information. These errors will inevitably impact the derived estimates of the circulation patterns which are usually obtained by estimating the geostrophic velocities relative to the level of no motion at 400–500 m (e.g. Morrison et al., 2012). In this regard, it is necessary to note that direct velocity observations in the Makarov and Amundsen Basins as well as along the Siberian continental slope demonstrate relatively strong (4–7 cm/s) currents at these depths (Pnyushkov et al., 2015).

Modeling studies (e.g., Maslowski et al., 2000; Zhang and Rothrock, 2003; Wang et al., 2014; Zhang et al., 2016; Wang et al., 2016) have the advantage of better dynamical consistency, but may suffer from uncertainties in the forcing fields and sub-grid parameterizations, resulting in a rather different and sometimes controversial representation of the water's properties and in estimating circulation in Arctic Ocean models (e.g. Stainer et al., 2004; Holloway et al., 2007; Aksenov et al., 2016).

In the present study, we make an attempt to combine observations with the dynamical constraints of a numerical model in the framework of the four-dimensional variational data assimilation approach (4dVar). The method (e.g., Le Dimet and Talagrand, 1986) provides a way of interpolating observations in space and time using the dynamical constraints of a numerical model. In particular, this approach allows a reasonably accurate reconstruction of the data-driven circulation on the shelves, where geostrophic currents cannot be estimated from temperature/salinity observation alone.

We reconstruct summer-fall PSAO circulations during four different periods, focusing on the comparison of the 2008 July-December circulation with the respective conditions reconstructed in the previous decades (1972–1978, 1989–1996, 1997–2006) which correspond to the periods of positive and negative AOO phases (Proshutinsky et al., 2015). The year 2008 was chosen due to the largest volume of observations collected, after the anomalous ice retreat of 2007. To assess interannual variations of the FW content, we also reconstructed July-December circulations for 2003, 2004, 2005 and 2006. A significant effort has also been made to validate the performance of the Pan-Arctic Ice-Ocean Modeling and Assimilation System (PIOMAS), whose solutions were used to initialize the 4dVar assimilation.

The paper is organized as follows. In the next section we describe the methodology and the data set that have been used. In Section 3, the PSAO circulations for two anticyclonic (1972–1978,

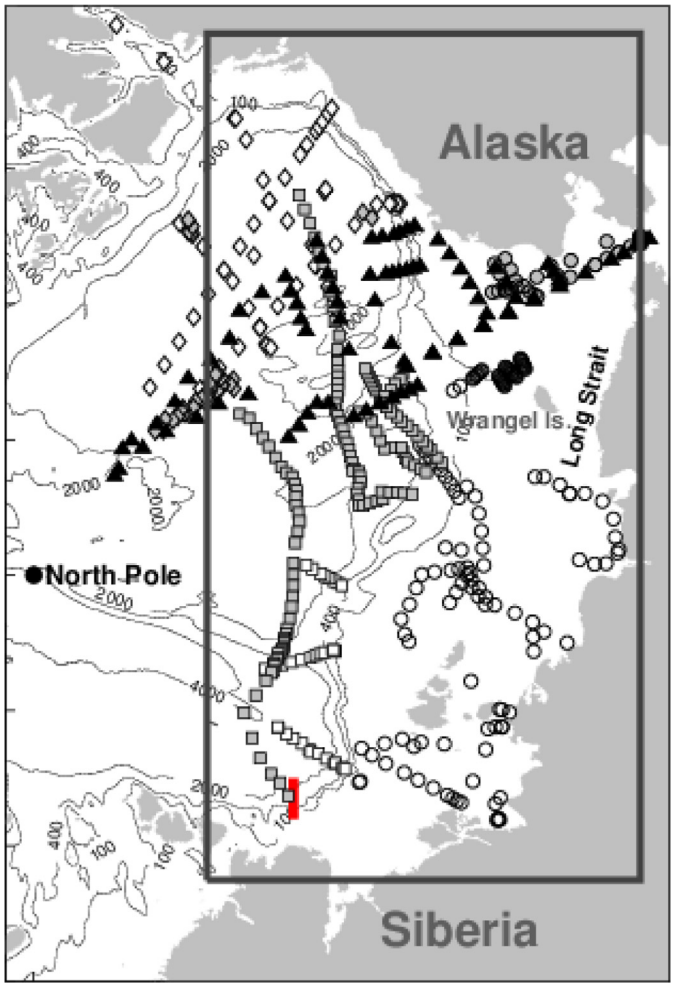

Fig. 1. PSAO model domain (solid rectangle) with hydrological stations assimilated into SIOM during July-December 2008 (http://oregon.iarc.uaf.edu/dbaccess.html). Contours show bathymetry. Vertical red line shows the Eurasian continental slope section where the flow of Atlantic water was monitored in the solutions. 2008 observation are designated by: (1) clear squares – CTD's from NABOS project; (2) clear circles – CTD's from Siberian Shelf Study; (3) clear diamonds – CTD's from BGEP; (4) gray squares – CTD from ARK23 PSA cruise; (5) gray circles – CTD's from Oshoru Maru cruise; (6) gray diamonds – ITP observations; (7) dark asterisk –ITP observations; (8) black triangles – CTD from the 2008 Chinese Arctic Research Expedition. (For interpretation of the references to colour in this figure legend, the reader is referred to the web version of this article.)

1997–2006) and one cyclonic (1989–1996) AOO periods are reconstructed and analyzed. Results of these reconstructions are used for analyzing the anomalous PSAO circulation during July-December 2008 retrieved from the synthesis of the IPY data with PSAO climatologies. A special focus is made on the quantification of the PSAO inflow at the Eurasian continental shelf break, on the advective FW transport into the Beaufort Gyre, and the validation of the reconstruction against independent SSH observations.

2. Methodology

The major objective of the present study is to investigate the details of the circulation within the PSAO domain (Fig. 1) during July-December 2008 and compare with the mean circulation patterns during three periods which correspond to different phases of the AOO and circulation during 2003–2006 in the same region. During 2003–2007, there was an intense accumulation of FW in the Beaufort Gyre. Starting in 2008 and the subsequent years following, the FW accumulation rates have dropped significantly (Proshutinsky et al., 2009; Zhang et al., 2016). Therefore, the circulation during 2008 can be treated as a typical circulation for a new period of the positive AOO. The second half of the year was selected as a testbed for analysis since data coverage during this time is much more abundant, which is crucial for a detailed reconstruction of the circulation features using a model-data synthesis technique. Also, July-December is a thermodynamically active period which sees a transition from peak ice melt to deep freeze in the upper ocean, and strong wind forcing which intensifies the vertical mixing and increases Ekman pumping processes.

In the presented analysis, we employ a methodology which has been successfully used by Panteleev et al., (2010; 2016) for reconstructing the circulation in the Chukchi and Bering Seas.

This was also applied for reconstructing the circulation in the entire Arctic Ocean (http://www.whoi.edu/science/PO/arcticgroup/projects/andrey_project2/resultsAP.html) at a coarser (65 km) resolution. The method is based on the successive use of two data assimilation systems: The first one, Pan-Arctic Ice-Ocean Modeling and Assimilation System (PIOMAS) assimilates ice concentration and sea surface temperature (SST) into a coupled ice-ocean model using a "sequential nudging" technique which attracts the model trajectory to observations, but, in contrast to 4dVar, disrupts the physics by introducing an artificial external forcing. Violation of the physical constraints may also cause improper spreading of the observational information in space and time. The PIOMAS model was chosen as one of the best models in simulating the water properties in the Arctic Ocean (Holloway et al., 2007).

The PIOMAS output provides realistic first guess estimates of the sea-ice and sea-atmosphere fluxes for the second assimilation system based on 4dVar assimilation into the semi-Implicit Ocean Model (SIOM). The second system makes adjustments to the poorly known model parameters (initial and open boundary conditions and surface flux estimates) in such a way that the model trajectory passes from observations at a distance consistent with their error bars.

2.1. Numerical models and data assimilation

Since a large part of the PSAO is ice covered during the second half of the year, the data assimilation procedure should take into account ice-ocean interactions, and the data assimilation algorithm should be designed for a sea ice/ocean coupled model. Development of a 4dVar data assimilation procedure for such a complex system is not straightforward. A strong nonlinearity of the sea ice dynamics complicates the development of a stable adjoint model and results in low controllability of the sea ice model. Effectively, dynamical complexity of this coupled ice-ocean system may limit the applicability of the 4dVar data assimilation methods for integration times longer than a month. Thus, to avoid such technical problems, we use a set of simplified suboptimal data assimilation methods described below.

2.1.1. PIOMAS

The PIOMAS system is a coupled parallel ocean and sea ice model with capabilities of assimilating sea ice concentration and SST data. It consists of the thickness and enthalpy distribution ice model developed by Zhang and Rothrock (2001; 2003) and the Parallel Ocean Program (POP) developed at the Los Alamos National Laboratory (Smith et al., 1992). The POP ocean model is an advanced version of the Bryan–Cox–Semtner-type ocean model (Bryan, 1969; Cox, 1984; Semtner, 1986). The POP includes many improvements: incorporation of the isopycnal mixing scheme of Gent and McWilliams (1990) and the K-profile parameterization scheme for vertical mixing (Large et al., 1994), implementation of an implicit free-surface formulation of the barotropic mode, and

adaptation to shared-memory or distributed-memory parallel computers (Smith et al., 1992). The sea ice model explicitly simulates sea ice ridging and has 12 ice categories, each for ice thickness, ice enthalpy, and snow. The model employs a teardrop viscousplastic ice rheology that determines the relationship between ice internal stress and ice deformation (Zhang and Rothrock, 2005). Assimilation of sea ice concentration in PIOMAS is based on sequential nudging of the model ice concentration estimate to the observed one in a manner that minimizes the effect of observational errors in the interior of the ice pack with reduced weighting of the observations (Lindsay and Zhang, 2006). Assimilation of SST is based on the nudging of the model's SST estimate to the NCEP/NCAR reanalysis SST, following Manda et al. (2005). The NCEP/NCAR reanalysis SST is based on the Reynolds SST analysis (Reynolds et al., 2002) which incorporates satellite and in situ observations (Kalnay et al., 1996). The SST assimilation is performed only in open water areas where satellite SST observations are available. More details on the PIOMAS assimilation run used in this study can be found in the paper by Zhang et al. (2015).

2.1.2. SIOM assimilation system

The 4dVar assimilation performed by SIOM is a much more computationally intensive procedure with the benefit of producing a dynamically consistent evolution of the ocean fields which is also consistent with the assimilated data. The SIOM dynamical core is a modification of the C-grid, z-coordinate OGCM developed in the Laboratoire d' Oceanographie Dynamique et de Climatologie (Madec et al., 1999). This model is semi-implicit in both barotropic and baroclinic modes, permitting long-term simulations with relatively large time steps of approximately 0.1–0.3 days. This design was specifically chosen to reduce the number of control parameters in the 4dVar runs involving long-term regional simulations primarily controlled by fluxes at the open model boundaries and the sea surface. More details of the SIOM data assimilation system can be found in Panteleev et al. (2006, 2010) and references therein.

The principal advantage of the utilized 4Dvar data assimilation approach, compared to the widely used optimal interpolation algorithm, is the possibility of being able to use observations taken during relatively long (~6 months) time intervals, where the 4Dvar approach implicitly employs inhomogeneous correlation functions defined by the model dynamics. The optimal interpolation approach uses heuristic approximations to the correlation functions because they cannot be obtained with sufficient accuracy from the available data.

SIOM 4Dvar data assimilation system was successfully applied for the reconstruction of the circulation in the regions heavily controlled by open boundary conditions (e.g. Nechaev et al., 2005; Panteleev et al., 2005, 2010, 2016). It was also used for the reconstruction of the climate circulation and corresponding mean dynamic ocean topography (Panteleev et al., 2007; 2011; 2014) and optimization of the observations through adjoint sensitivity analysis and observing system simulation experiments (Panteleev et al., 2008, 2013).

2.1.3. Configuration of the assimilation systems

The PIOMAS ice-assimilative run was performed for the entire Arctic domain (north of 43°N) during 1972–2008. Fig. 2 shows the bi-monthly averaged PIOMAS solution during the second half (July-December) of 2008. Comparison with the direct velocity measurements from moorings along the Siberian continental slope demonstrates only a qualitative agreement of this solution with the data. Despite the presence of a small westward component along the continental slope in the mean model velocities, these are barely consistent with observations in direction and magnitude (lower panels in Fig. 2). Similarly, the respective SSH patterns (upper panels in Fig. 2) are only in qualitative agreement with the monthly DOT distributions, recently developed by Armintage et al. (2016), whereas their magnitude appears to be substantially underestimated (see Section 3.2.2).

These inconsistencies were substantially reduced by 4dVar corrections of the model's initial state and its surface/boundary forcing. The PIOMAS run was used as a first guess approximation to the above mentioned model controls of the SIOM 4dVar system that was run in the PSAO domain (Fig. 1) for 6-month intervals corresponding to the mean PSAO variabilities for the years 1972–1978, 1989–1996, 1997–2006, and for its (data-driven) evolution in 2008.

The SIOM 4dVar system was configured with a horizontal resolution of 27 km with 30 unequally spaced vertical layers ranging in thickness from 5 m near surface to 600 m near the bottom. The time step of the model was 0.2 days. With this discretization for a 6-month run, the number of unknowns at the lateral open boundaries was close to 7 million, greatly exceeding the number of available observations (see next section) and formally making the 4dVar problem under-determined. To relax this condition, the temporal variability of the SIOM forcing fields at the open boundaries was approximated by piecewise linear functions of time on 10-day intervals, thus reducing the number of unknowns $10/0.2 = 50$ times.

The final product of the PIOMAS/SIOM data assimilation system were the oceanic fields of temperature T, salinity S, horizontal velocities u, v and sea surface height ζ sampled on the SIOM regular grid at a 10-day discretization during a 6-month period.

2.2. Data and data sources

2.2.1. Surface fluxes

Near surface (10 m) wind fields, heat and salt fluxes were taken from the National Centers for Environmental Prediction (NCEP) reanalysis (www.cdc.noaa.gov/cdc/data.ncep.reanalysis.derived.html). The corresponding momentum flux was recalculated from the NCEP wind using the conventional bulk formula (Large and Pond, 1981). To allow for the adjustment of the spatial details in the model forcing, we used wind stress, heat, and salt flux data with relatively high error variances (up to 40% of their spatial and temporal variability). Meteorological data were filtered with a 5-day cutoff filter in order to remove high-frequency variations. In the ice-covered regions, the 4dVar DA subsystem used the ice-water surface fluxes delivered by the PIOMAS system.

2.2.2. Satellite observations

Sea ice concentration included the Special Sensor Microwave/Imager (SSMI) ice concentration obtained from the Hadley Center (http://hadobs.metoffice.com/hadisst/) and interpolated on the PIOMAS model grid. To validate PIOMAS ice cover performance, we used raw buoy displacement data from the International Arctic Buoy Program (IABP) and satellite-derived ice velocities based on images from the SSMI, available from the National Snow and Ice Data Center (NSIDC). In addition, sea ice concentration data were used as proxy data for sea surface temperature, which was assumed to be near the freezing point for the particular near surface model salinity.

Sea Surface Temperature NCEP/NCAR daily SST data (https://www.esrl.noaa.gov/psd/data/gridded/data.noaa.oisst.v2.html) were used in the PIOMAS data assimilation system. A comparison of the NCAR/NCEP SSTs and in situ historical surface temperature observations (see description below) in the PSAO region were fairly consistent and had standard deviations of 0.5 °C–0.7 °C, depending on the period of time. In the 4dVar DA system, we used the Operational SST and Sea Ice Analysis (OSTIA) product

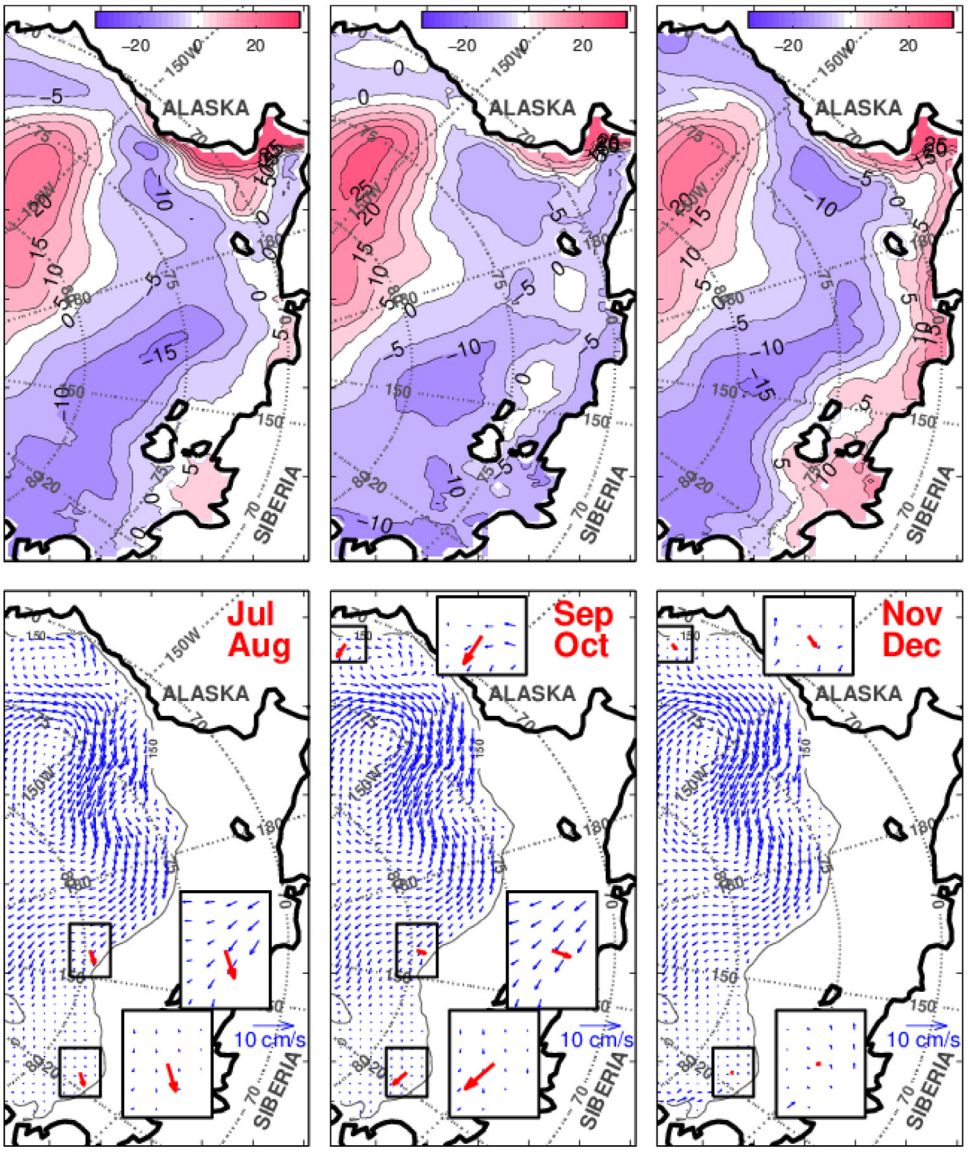

Fig. 2. Bi-monthly (Jul-Aug, Sep-Oct, Nov-Dec) averaged PIOMAS SSH (cm, upper panels) and circulation (lower panels) in 2008. Red arrows in boxes show mean velocities measured by NABOS moorings during the respective periods. (For interpretation of the references to colour in this figure legend, the reader is referred to the web version of this article.)

(Strak et al., 2007; Donlon et al., 2012), which appears to show better consistency with in situ SST observations in the PSAO (Stroh et al., 2015). These data were used with a 0.5°-2.5 °C STD.

Sea Surface Height data were employed in the present study only for validation purposes. Two satellite altimetry products were used. The first one was the AVISO along track Envisat altimetry observations available from http://www.aviso.altimetry.fr/en/my-aviso.html. The preprocessing of these data was performed in three steps: First, the mean along track satellite altimetry anomalies were computed as a time average over the ice-free (July-September) periods encompassing twelve 35-day cycles in 2003–2006 and two 35-day cycles in 2008. Second, the obtained along-track SSH anomalies were averaged within 20 km x 25 km bins. Finally, the SSH anomaly values were low pass filtered with a decorrelation scale of 50 km and interpolated onto the SIOM grid to obtain the 2003–2006 and 2008 July-September SSH anomalies in the region. The difference between 2003–2006 and 2008 SSH anomalies was used for the evaluation of the reconstructed 4Dvar SSH in order to remove possible inaccuracies in definition of the reference Mean Dynamic Ocean Topography utilized by AVISO to recalculate SSH anomalies into absolute SSH.

Note however, that the relatively small ensemble used for the computation of the PSAO SSH anomalies is likely to result in substantial errors, especially in the shallow water regions where SSH varies significantly due to tides, winds and topographically trapped waves (e.g. Schlax and Chelton, 1994a; 1994b).

Since Envisat (AVISO) observations are available only in the ice-free subdomain of the PSAO, which covers less than 20% of the space-time volume of the 2008 4dVar reconstruction, we also employed an alternative Dynamical Ocean Topography (DOT) product developed recently by Armitage et al., (2016). This dataset includes monthly mean DOTs between 60°N-81.5°N for the period of 2003–2014. This product was obtained as a composite of along-track altimetry observations from the Envisat satellite referenced to the GOCO03 geoid and the SSH derived from CryoSat-2 observations (Laxon et al., 2013). CryoSat-2 data were used for estimating SSH in the leads and polynyas over areas with dense ice coverage. The final DOT was averaged over the 2°x0.5° grid cells and then the gridded data were additionally smoothed with a Gaussian convo-

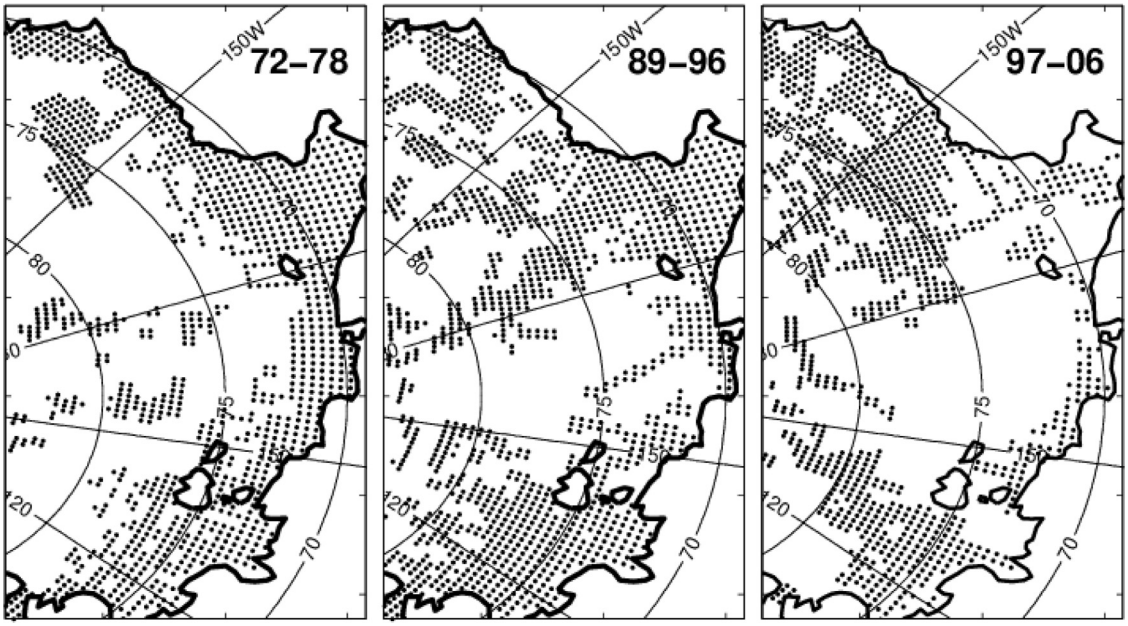

Fig. 3. Spatial distribution of the AARI data during three multi-year assimilation periods http://www.whoi.edu/science/PO/arcticgroup/projects/andrey_project2/resultsAP.html.

lution filter with a radius of 300 km (Armitage et al., 2016). As a result of the smoothing, the final product can be used only for the validation of the large scale component of the PSAO circulation. In further discussion, we will refer to this DOT product as CPOM-DOT.

2.2.3. In situ observations

Hydrological data from the database of the Arctic and Antarctic Research Institute, St. Petersburg, Russia, (AARI) was a major source of information for the SIOM 4dVar assimilation during the 1972–2006 period. The AARI database comprises of more than 600,000 profiles obtained by the research vessels of AARI and other institutions during the period of 1900–2006. Previously, the data from the AARI database were assimilated into the coarse (65 km) resolution SIOM-PIOMAS data assimilation system and utilized for the reconstruction of the annual mean Arctic Ocean states for three multi-year intervals: 1972–1978 (hereinafter A1), 1989–1996 (C1), and 1997–2006 (A2). Results of this reanalysis as well as AARI data can be found at http://www.whoi.edu/science/PO/arcticgroup/projects/andrey_project2/resultsAP.html. In the present study, these coarse resolution states were interpolated on a finer (27 km) grid and utilized as background fields for the reconstruction described in Section 3.1.

Assimilation of the raw temperature and salinity (*TS*) profiles from the AARI database into the model is not computationally efficient since, in many cases, the individual instantaneous profiles were located close to each other in either space or time, so that the respective space-time intervals could not be resolved by the assimilative models run at a coarser resolution. To prepare these data for 4dVar assimilation, they were preprocessed as follows. First, the profiles within a given month were grouped into regular 25–25 km bins, and the data within each space-time bin were linearly projected onto PIOMAS levels. These data were then averaged in time over the monthly period of the bin and the corresponding error bar was estimated for subsequent use in the 4dVar data assimilation procedure. The number of *TS* profiles in some model grid boxes was not sufficient enough to derive reliable estimates of the error variance. For these cases, horizontal interpolation of the statistics characterizing data variability was carried out. The outlined procedure was executed for each of the three multi-year intervals 1972–1978 (hereinafter A1), 1989–1996 (C1), 1997–2006 (A2) and for each year during the 2003–2006 period. Fig. 3 shows the coverage of the first three climatological periods by the AARI data points. These data were assimilated by the SIOM 4dVar system using a bilinear grid-to-grid interpolation. A similar preprocessing of the AARI observations was utilized for the analysis of the Kara Sea circulation by Panteleev et al. (2007).

Bering Strait transport estimates were taken from the results of the interdisciplinary monitoring program (Woodgate et al., 2006; R.A. 2015) based on observations at the A3 mooring located 27 km north of the Diomede Islands (Woodgate et al., 2007). Accurate representation of the Bering Strait flow requires a resolution higher than 27 km and an extended model configuration which would include the entire Arctic and North Pacific Oceans, which is not computationally feasible for 4dVar reanalysis. Therefore, the observations of the Bering Strait transport were particularly important as they controlled the overall transport of mass and freshwater from the Pacific Ocean, and therefore imposed constraints on the net outflow of the PSAO waters into the Atlantic. For the assimilation periods before 1991, we used the climatological monthly mean Bering Strait volume transports compiled by Woodgate et al. (2005).

2008 hydrography included additional data sets from the International Polar Year (IPY) database compiled by Stroh et al. (2015) (http://oregon.iarc.uaf.edu/dbaccess.html). These observations included 533 instantaneous *TS* profiles from a variety of sources, including 82 stations from the 2008 Chinese Arctic Research Expedition (Zhang, 2009); 133 profiles from the Eurasian shelf obtained during the course of the Siberian Shelf Study (http://www.iarc.uaf.edu/research/projects/siberian-shelf-study); 45 ice-tethered profiler observations released by the BGEP of the Woods Hole Oceanographic Institution (Krishfield et al., 2006, http://www.whoi.edu/page.do?pid=20781); 73 CTD profiles from the BGEP expedition in 2008 (http://www.whoi.edu/beaufortgyre); 65 profiles obtained during the 2008 expedition in support of the Nansen and Amundsen Basins Observational System (NABOS); 58 CTD profiles from the Hokkaido University expedition onboard the RV Oshoru Maru (http://odyssey.fish.hokudai.ac.jp/IPY/data2008/CruiseReportSummary-2008.pdf); and 142 profiles acquired during the ARK23 PSA cruise on the German r/v Polarstern (https://www.pangaea.de/PHP/CruiseReports.php?b=Polarstern). Locations

of the above listed IPY hydrographical observations are shown in Fig. 1. The estimated T&S variances vary from region to region within the limits of 0.1 °C – 0.3 °C and 0.03–0.2 psu, respectively. These data provided a key contribution to constraining the 2008 PSA circulation and allowed for confident identification of the major anomalies in the evolution of the ocean state.

3. Results

3.1. 1972–2006 circulations

In order to reconstruct the mean July-December PSAO circulations during two anticyclonic (A1 (1972–1978), A2 (1997–2007)) and one cyclonic (C1 (1989–1996)) phases of the AOO, three half-year 4dVar assimilation runs were performed for the A1, A2 and C1 periods. The 6-month averages of the respective circulations are presented in Fig. 4.

Anticyclonic AOO phases (A1, A2) are characterized by a more pronounced BG with maximum SSH values of 18 and 16 cm, respectively. The center of the Gyre is located around 80°N 155°W during the A1 phase. In the next anticyclonic phase, it displaced approximately 5° degrees southeast. The SSH pattern during C1 (middle panel in Fig. 4) does not show a pronounced offshore anticyclonic dome, indicating that FW accumulation in the Beaufort Gyre was at a relaxed phase. These features appear to be in reasonably good agreement with the conceptual theory and analysis of the hydrological observations conducted by Proshutinsky and Johnson (1997) and Proshutinsky et al. (2002, 2009).

The pronounced SSH depression with the minimum at 110°E (upper panels in Fig. 4) is a surface signature of the AW inflow, whose pathway generally follows the Eurasian continental shelf break at this longitude with the core at 150–500 m. Our results indicate a general increase of the total transport in this region from 2.1 Sv (A1) to 1.5 Sv (C1) to 2.8 Sv during A2. The observations of the AW flow through the Fram Strait are available only since 1997. Taking into account the lagged correlation between along-slope flows in the Fram Strait and the Laptev Sea (e.g., Dmitrenko et al., 2008a), and suggesting that mean during 1997–2010 is within the upper estimate of the mean climate flow through the Fram Strait, our result show no contradiction with the findings of Beszczynska-Moller et al. (2012), who observed an increased AW volume transport (~7.1 Sv) through the Fram Strait during 1997–2006.

It is worth noting that during the A1 and A2 phases, the above mentioned SSH depression is more profound, while during the C1 phase, it was divided by the saddle around 75°N (middle upper panel in Fig. 4). Taking into account that the mean flow through the Bering Strait is due to the large scale SSH difference between the Arctic Ocean and the Bering Sea, one can speculate that the positive AOO phases tend to support intensification of the Bering Strait throughflow. This proposition is qualitatively supported, or at least does not contradict the SSH values of −7, −1 and −3 cm averaged over the area in the Northern Chukchi Sea (upper panels of Fig. 4). However, the available SSH observations in the Bering Strait and the Beaufort Sea do not span enough time back to 1980-s and 1970-s to confirm this result.

Fig. 4 also indicates that the fresh Siberian shelf water tends to accumulate west of the Wrangel Island during the cyclonic phase (C1) causing amplification of the anticyclonic dome in the East Siberian Sea (ESS) around 73°N 150°E (Fig. 4, middle upper panel). This water has a tendency to be released through the Long Strait separating the Wrangel Island from the continent with approximate transports of 0.03, 0.12 and 0.09 Sv during the A1, C1 and A2 phases, respectively. These numbers suggest a presence of the developed Siberian Coastal Current which brings diluted waters from the East Siberian Sea into the Chukchi Sea (Weingartner et al., 1999). The inverse modeling of the southern Chukchi Sea conducted by Panteleev et al. (2010) suggests that this pathway is usually more persistent in the summer and weakens during the fall and winter months with a decline in the Siberian river runoff.

In summary, the data assimilation results indicate certain alterations of the PSAO state in response to the changes induced by the AOO. The periods of positive AOO index favors BG amplification accompanied by an offshore displacement and by a certain increase of the Bering Strait transport. During the periods of the negative AOO index, the Beaufort Gyre has a tendency to move closer to the coast, whereas the ESS circulation forms an anticyclonic dome in the SSH field with increased FW content (3700 km^3 for both A1 and A2 and 4200 km^3 for C1). The estimates of the total FW content calculated for the BG region (shown in Fig. 9) are 17,500 km^3, 19,200 km^3 and 18,500 km^3 for the A1, C1 and A2 periods. Taking into the account the difference in the region and data processing methodologies, these numbers appear to be in reasonable agreement with the estimates of Proshutinsky et al. (2009).

3.2. Circulation features in 2008

3.2.1. 2008 circulation and SSH patterns

The reconstructed bi-monthly evolution of the SIOM 4Dvar SSH and circulation at 250 m during July-December 2008 is shown in Fig. 5. The SSH patterns are characterized by a pronounced BG dome which gets slightly stronger in November-December (right panel in Fig. 5) attaining a 40 cm elevation in the center. Compared to the relatively smooth and symmetric SSH derived through optimal interpolation (e.g. McPhee, 2013), the reconstructed SSH in the BG reveals finer features consistent with the observations. During September-October, the SSH pattern is characterized by a secondary SSH maximum at 74°N 140°W which tends to erode by the end of the year but still persists as a tongue spreading towards Alaska, along 140°W. This feature is seen in the AVISO anomalies averaged over the second half of 2008 (see Section 3.2.2). Another prominent feature consistent with the CPOM-DOT monthly distributions, discussed below, is the prominent thorough spreading zonally in the latitude band between 72°N-80°N from Severnaya Zemlya to the Bering Strait. Its signature is also present in the PIOMAS solution (Section 2.1.3) and is a natural result of the dynamically constrained assimilation of the hydrographic data underlying the reconstruction. A prominent signature of this SSH depression can also be identified in the upper left and right panels of Fig. 4 corresponding to the anticyclonic phases of the AOO index.

We assume that the emergence of this depression could be one of the causes of intensification of the Bering Strait transport due to the increase of the large-scale sea level difference between the Chukchi and Bering Seas. This is supported by the analysis of Woodgate et al. (2012) who estimated the balance of the forces controlling the flow through the Bering Strait and found a significant increase of the pressure head in 2007–2011 with respect to the 1997–2006 period (Fig. 1h from Woodgate et al., 2012), when the Bering Strait transport was smaller.

Interestingly, a similar behavior of the SSH “depression” is observed in the bi-monthly SSH fields averaged over the area north of the Bering Strait (upper panels in Fig. 5) which were estimated to be −11, −10, and −6 cm respectively, which is consistent with the decline of the Bering Strait inflow from 1.1 Sv in July-August to 0.5 Sv in November–December 2008 (Woodgate et al., 2012). A general tendency for the decrease of the Bering Strait transport in fall-winter months was also described by Roach et al. (1995), and Woodgate et al. (2005, 2007).

The SSH depression in the Arctic Ocean is not the only factor controlling the Bering Strait flow. The SSH distribution in the Bering Sea as well as the regional wind forcing should obviously play a role. Thus, a more accurate analysis of the impact of the pressure head forcing on the flow through the Bering Strait needs

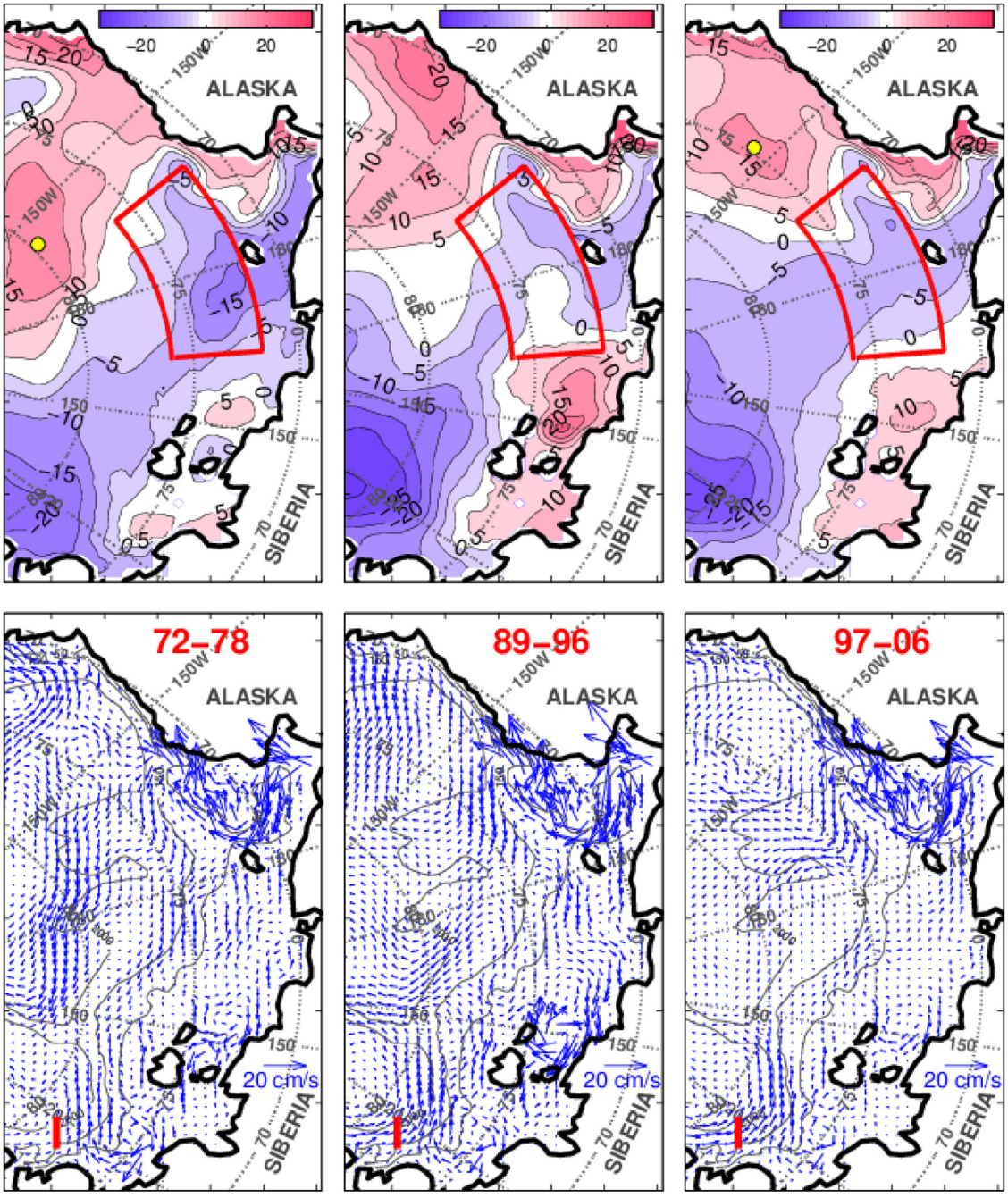

Fig. 4. The mean SSH (cm, upper panels) and surface velocity (cm/s, lower panels) fields corresponding to the three phases of the AOO: A1 (1972–1978), C1 (1989–1996) and A2 (1997–2006). The red vertical line near 120°E indicates the section across the continental shelf break where the total transport has been computed. The SSH averaging area is marked by the red rectangular sector. Yellow circles denote the BG center locations. (For interpretation of the references to colour in this figure legend, the reader is referred to the web version of this article.)

a higher resolution data assimilation system that includes both the Bering Sea and PSAO region.

Of particular interest is the impact of the above mentioned SSH depression on the transport pattern in the region of the AW inflow. During the summer (i.e. July-August 2008), the negative SSH anomaly is closely attached to the coastline, creating a positive SSH gradient across the continental slope and a westward geostrophic transport of −2.9 Sv along the continental shelf break (lower left panels in Fig. 5). The effect becomes less visible by the end of the year as the negative SSH anomaly detaches from the continental slope and the total transport relaxes to eastward values of 0.8 Sv and 1.0 Sv, respectively for the September-October and November-December periods. The diagnosed flow reversal agrees well with the NABOS moored velocity observations available at http://nabos.iarc.uaf.edu/data (red arrows in Fig. 5, see also Fig. 4 from Pnyushkov et al., 2015), that were *not used* for constraining the optimal 4dVar solution.

Interestingly, during July-August (and to some extent during September–October), the reverse flow can be traced along the entire Siberian continental slope. This westward flow weakens in September–October but can still be observed along the continental slope west of 180°E. A signature of the weak westward flow is also evident in the PIOMAS solution (Fig. 2) obtained without the assimilation of the hydrography. One may speculate that pre-

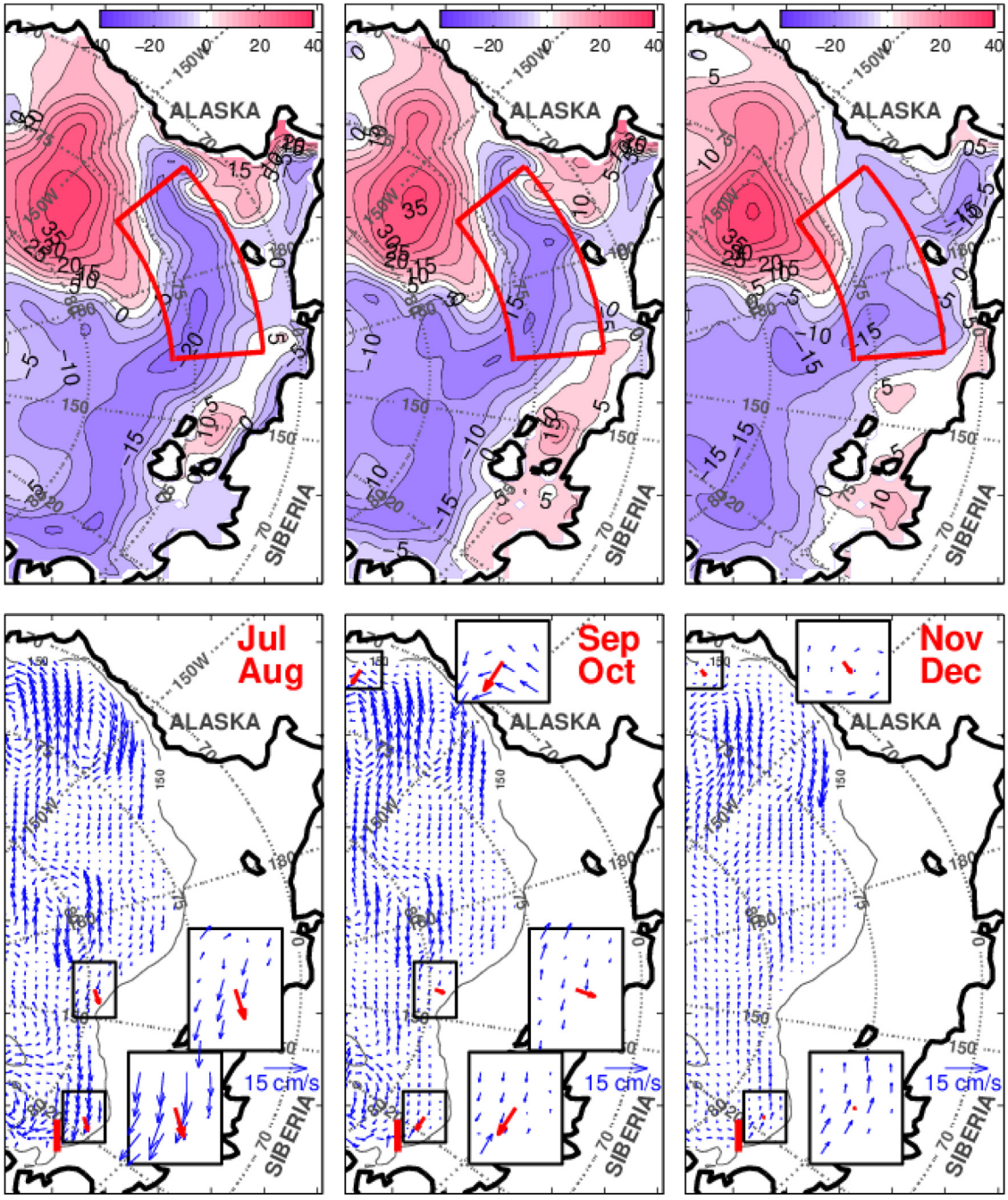

Fig. 5. The fields of 2008 bi-monthly averaged SSH (cm, upper panels) and velocity at 250 m (cm/s, lower panels). NABOS moorings with the respective velocity observations are shown in the inserts. The section used for calculating the total transport in the AW inflow region is shown by the thick red line. The solid rectangular sector in the upper panels shows the SSH averaging area is used for assessment of the Bering Strait transport variability. (For interpretation of the references to colour in this figure legend, the reader is referred to the web version of this article.)

conditioning by the anomalous large-scale atmospheric forcing, in the previous years, is a major factor causing the anomaly which was made more prominent by the 4Dvar assimilation of the hydrographic data that keeps memory of the atmospheric conditions in the preceding years.

Another important feature associated with the SSH depression is a significant amplification of the eastward shelf current carrying relatively FW enriched by the Siberian river's runoff. This current has a typical velocity of 0.1 m/s with a capability of FW transport for several hundred kilometers during the summer season. More importantly, is this current reduces the transport time of the Eurasian shelf water to the Bering Strait meridian by almost two times, as it takes a much shorter route north of the Wrangell Island. In the absence of the depression, the FW pathway mostly goes through the Long Strait, which penetrates much deeper into the southern Chukchi Sea and requires a much longer time (~1 year) to be a part of the anticyclonic circulation associated with the Beaufort Gyre. In principle, this effect may partly contribute to the freshening of the Beaufort Gyre described by Morison et al. (2012), but, as it will be shown below, this contribution is likely to be negligible in the currently observed process of the FW accumulation.

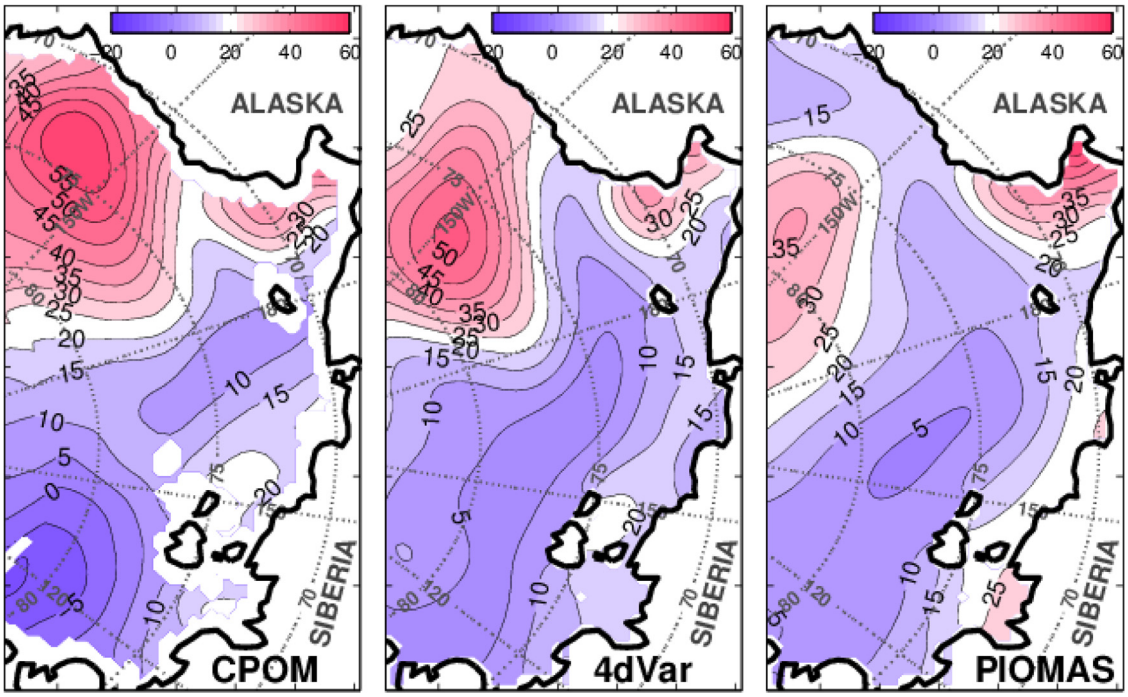

Fig. 6. Averages of the CPOM-DOT (left), 4dVar (center) and the PIOMAS SSH during September-October 2008.

3.2.2. Validation against SSH data

Since satellite altimetry observations in the Arctic are relatively scant and inaccurate due to the presence of ice, we did not use them directly in the reconstruction. Upon the completion of this study, a new CPOM-DOT product (Armitage et al., 2016) combining Envisat and CryoSat observations and referenced geoid became available. Although CPOM-DOT has a relatively coarse resolution in time (1 month) and space (more than 300 km), it is formally free from ice-cover restriction of the AVISO, and turns out to be valuable for the validation of large-scale SSH features in modeling and assimilation results.

Fig. 6 compares CPOM-DOT, 4dVar and PIOMAS SSH patterns averaged for September–October of 2008. PIOMAS and 4Dvar solutions were additionally smoothed with a low-pass filter in order to be consistent with the CPOM-DOT horizontal resolution. The 2008 CPOM-DOT pattern has two major differences with the CPOM-DOTs in the previous years (2003 is shown as an example in Fig. 7). First, the 2003 SSH depression extending from 80°N 110°E toward the Siberian Coast near the Wrangel Island, continues further east toward the Alaskan Coast, in 2008. The second difference is the much stronger Beaufort Gyre in 2008.

In 2008, the BG magnitudes in the CPOM-DOT and 4Dvar SSH patterns are very close (55 cm and 50 cm, respectively). However, the BG center in the CPOM-DOT is approximately at 74°E 143°W, while the 4Dvar SSH has a maximum at approximately 77°N 154°W. It should be noted, however, that the BG position in the 4dVar reconstruction is in almost perfect agreement with the results of hydrographic data analysis by McPhee et al. (2009), who diagnosed the 2008 BG center position at 75.8°N 153°W. A more recent analysis of the CPOM-DOT product by Armintage et al., (2017) also indicates a certain north-western drift of Beaufort Gyre center after 2008.

Comparison of the SSH distributions during 2003–2006 demonstrates a much better similarity between the CPOM-DOT and 4dVar SSH, with correlation coefficients between the SSH patterns ranging within 0.92 (2003) and 0.96 (2006). Also noteworthy, is that the 2003 pattern is shown to be qualitatively similar to the one diagnosed for the A2 period (1997–2006, Fig. 4 upper right panel). This similarity indicates that the major anomalies observed in 2008 were taking place either near the very end of the A2 period (2005–2006), or even into 2007–2008. Note also, that the 2008 CPOM-DOT minimum around 80°N, 120°E (Fig. 6, left panel) is not consistent with the NABOS velocity observations shown in Fig. 5. To some extent this could be attributed to a relatively low horizontal resolution of the product (note that the smoothed 4dVar and PIOMAS patterns in Fig. 6 also significantly decreases the SSH signature of the westward flow along the continental slope in the western Laptev Sea.

Overall, taking into account the possible errors associated with the limited set of the Envisat observations and significant smoothing of the CPOM-DOT, we may assume that the presented 4dVar reanalysis is in satisfactory agreement with the CPOM-DOT product.

As expected, comparison with the higher-resolution and "ice-free limited" AVISO data bears less similarity with the 4dVar reconstruction (Fig. 8). The preprocessed (see Section 2.2.2) along-track AVISO altimetry appears to have significant (0.78) correlation with 4dvar only in the region deeper than 100 m, while showing evidence of a secondary BG dome around 73°–74°N 140°W (see Section 3.2.1) and clear signatures of the BG southern periphery along 76°N and between 180°–150°W. Correlations with AVISO are not as good further south due to a loss of accuracy at the shelves caused by contamination of the signal by tides, coastally trapped waves, and insufficient statistics. The major reason for poor statistics is that although the satellite altimetry observations in the Arctic Ocean are spatially accurate enough (3–5 cm) starting with the launch of Envisat (2003–2011) and Saral (2014-present) missions, the temporal sampling is not. This is due to the relatively long (35 days) repeat cycle of these satellites and ice coverage during most of the year, where there are only about 20–30 accurate altimetry observations for each Envisat track in the PSAO region since 2003. Such a small ensemble may significantly increase the residual error in the SSH anomaly estimates, especially in the shallow shelf regions abundant in the Eurasian sector. Taking all these consider-

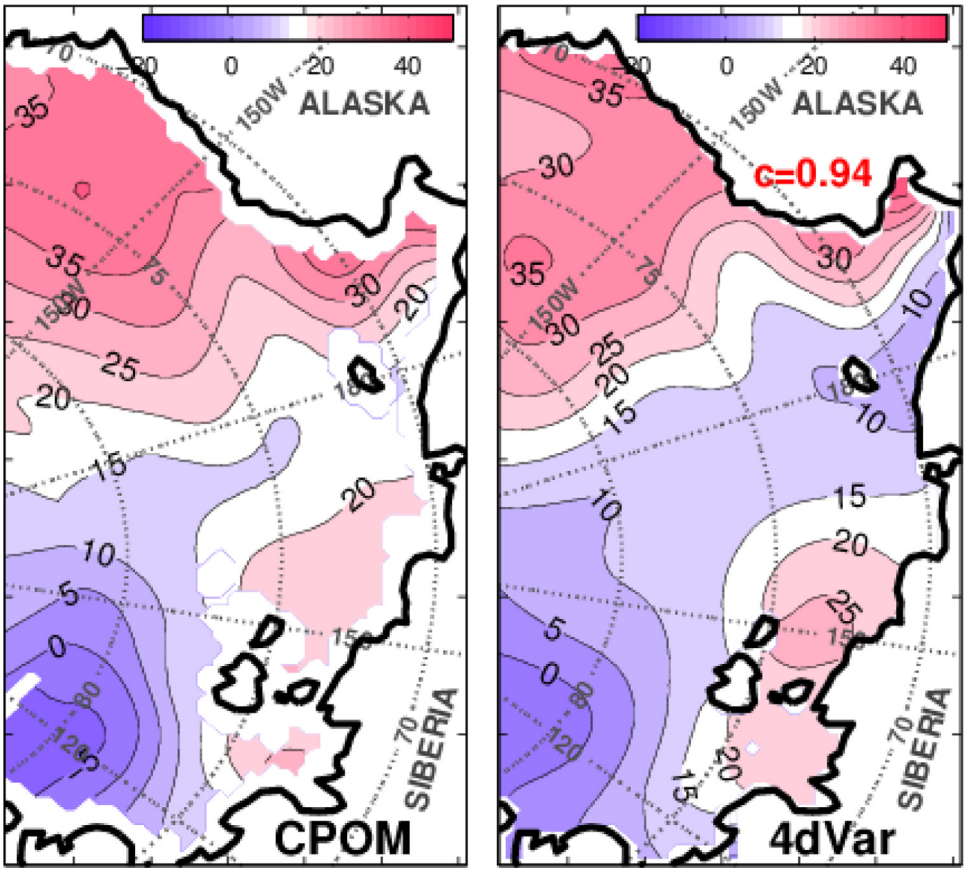

Fig. 7. Bi-monthly average of the CPOM-DOT (left) and the corresponding 4Dvar SSH (right) during September-October 2003.

ations into account, we assume that the correspondence between the SSH patterns in Fig. 8 is also satisfactory.

3.3. Freshwater content

The understanding of the processes controlling the FW content in the Arctic Ocean is an important question which brings a lot of attention to the Arctic research community. The FW content in the water column was estimated via the relationship (e.g. Proshutinsky et al., 2009):

$$\mathrm{FW} = \int_{z^*}^{0} \left[1 - \frac{S(z)}{S_{ref}}\right] dz$$

where the reference salinity $S_{ref} = 34.8$ psu, $S(z)$ is the salinity of the water at depth z and z^* is defined as either bottom or the depth where $S(z) = S_{ref}$ while $z = 0$ corresponds to the ocean surface.

The 4dVar FW content in 2008 clearly demonstrates a significant FW accumulation in the BG in 2008 as compared to the preceding decade (Fig. 9). Location of the 2008 maximum is in good agreement with the results of McPhee et al. (2009).

Apart from the increase of the net FW content in 2008, comparison with the mean FW distribution in 1997–2006 indicates a north-westward shift in the location of the FW maximum from 74°N 145°W to 71.5°N 155°W. This agrees well with the FW maps derived by Proshitinksy et al. (2009). The total freshwater content within the volume bounded by 70.25°N-80°N, 170°W-140°W, and depths less than 400 m within the 4dVar model boundaries was found to be about 20,700km^3 and 18,500km^3 for 2008 and 1997–2007, respectively.

The estimated total FW content for 2008 is slightly (5%–6%) smaller than that found in literature (e.g. http://www.whoi.edu/website/beaufortgyre/results). This is due to a somewhat smaller area of the integration of the 4dVar solution and the off-shore displacement of the BG observed in 2008.

To assess interannual evolution of the BG FW content, we calculated this quantity for 2003, 2004, 2005 and 2006 within the same region. The results demonstrate its gradual increase from 16,700 km^3 in 2003 to 20,700 km^3 in 2008, and are close to the estimates of Proshutinsky et al. (2009). Note that in reality, the FW accumulation in the Beaufort Gyre in 2008 is probably even higher because of the integration area of the 4dVar domain, which does not include the entire BG. It is also worth mentioning, that the 4dVar FW content in the ESS did not change in 2003–2006 but did increase significantly (25%) in 2008 to attain the value of 4600 km^3. This agrees well with the abnormally high Lena River discharge in 2008 (annual discharge 716km^3) (Charkin et al., 2011).

To assess the FW origin accumulated in the BG, the FW transports across the three sections shown in Fig. 9 were calculated for each year and then averaged within respective 6-month periods. According to these results (Fig. 10) the FW inflow through the southern boundary does not vary significantly in time, remaining around -0.1 ± 0.02 Sv, and slightly decreases after 2006, while the FW transport through the eastern section persistently increases with an outflow of -0.1 Sv in 2003 and an inflow of 0.08 Sv in 2008. The FW transport through the western section varies, with a 0.01 Sv inflow during 2003–2004 and approximately a 0.1–0.15 Sv outflow during 2006–2008.

These numbers indicate that during 2003–2004 (and probably earlier), the increase of the BG FW content was mostly due to the advective FW transport across the southern boundary (presumably water from the Chukchi and ES Seas), with a lesser contribution from the western section (presumably water from central Arctic

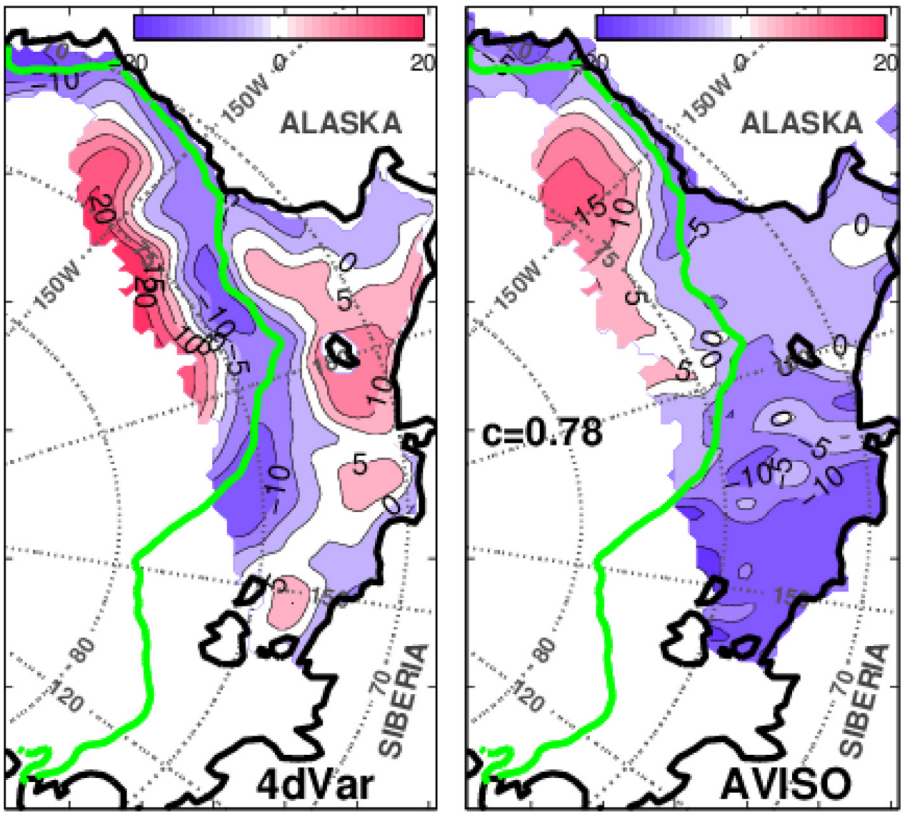

Fig. 8. A 4-month (July-October) average of the optimized SSH anomalies in 2008 (cm, left panel) with respect to the mean 4Dvr SSH in 2003–2006 and respective AVISO anomalies (right panel).
AVISO anomalies have been smoothed in accordance to the spatial resolution of the 4dVar system. Correlation coefficient for the off-shelf (deeper than 150 m) subdomain is shown by the green contour which is given on the low end of the AVISO panel. (For interpretation of the references to colour in this figure legend, the reader is referred to the web version of this article.)

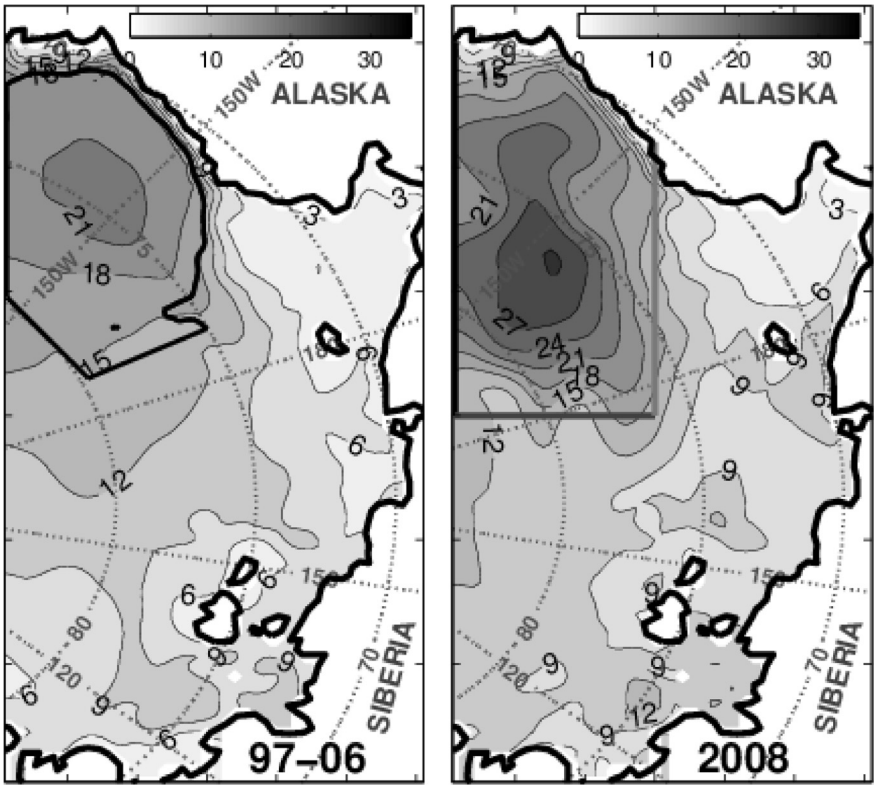

Fig. 9. Maps of the average FW content (m) of the 4Dvar reconstruction during September-October 1997–2006 and 2008. The three gray lines in the right panel show the eastern, western and southern sections used for estimating the FW transports.

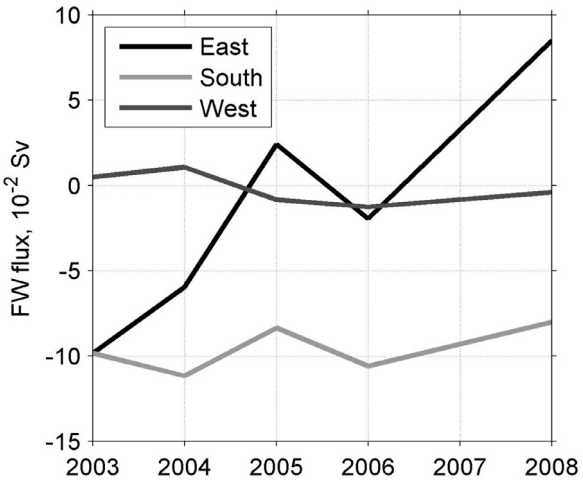

Fig. 10. The interannual variation of the mean FW transports during July-December 2003–2008 through the three boundaries of the Beaufort Gyre. Line colors correspond to the coloring in Fig. 9.

Ocean), and a minor outflow through the eastern section. This pattern drastically changes after 2006, when the western boundary became the major supplier of FW into the BG. The results indicate that the observed changes in the BG FW content were generally caused by the FW transport changes confined to the latitude band of 72°N-77°N at the eastern boundary of the 4dVar domain. The model domain does not allow backtracking of the water entering through the eastern boundary, but the hydrographic changes observed in the Lincoln Sea by De Steur et al. (2013) allows us to suggest that the source of the FW could be located north of the Canadian Archipelago or even near Greenland.

3.4. Lagrangian analysis

To highlight and further evaluate the potential impact of the anomalous features of the 2008 circulation with respect to the circulations from previous years, we conducted a Lagrangian analysis of the particle trajectories released in four regions: north of the Bering Strait, northeast of the Wrangel Island, in the western ESS, and in the region of the AW inflow. The experiments were conducted using the velocities averaged over the climatological periods of 1972–1978, 1989–96, and 2008. The respective 6-month trajectories are shown in Fig. 11. During 1972–1978 and 1989–96, the particles released in the region of the AW inflow traveled persistently eastward.

The left and central panels in Fig. 11 indicate that the 6-month particle trajectories released at the AW inflow near 110°E penetrate further eastward during the negative AOO index (1989–96), indicating a certain suppression in the AW inflow during the positive AOO phase in 1972–1978. The anomalous 2008 circulation which corresponds to the extended positive AOO period is characterized by a westward transport of the particles released along the continental slope and an eastward transport over the shelf. Taking into account the observational evidence of the AW propagation along the continental slope (Dmitrenko et al., 2008a), may suggest that reversal of the AW flow along the continental slope will result in the lesser penetration of the AW into the Canadian Basin and accumulation of the AW in the Eurasian part of the Arctic Ocean.

Particles released in the ESS during the periods of negative AOO (1989–96) demonstrate confinement of the trajectories within the ESS shelf, accumulation of additional FW and more intensive East Siberian coastal current transporting FW toward the Chukchi Sea through the Long Strait. In 2008, there is a clear tendency for the shelf water particles to follow the pathway north of the Wrangel Island, which allows some of them to enter the BG periphery in the same season (right panel in Fig. 11). However, after reaching the area with coordinates 74°N 160°W, these particles turn eastward. Thus, they do not affect the FW content in the area shown by the solid line in Fig. 11 and are conventionally utilized for the analysis of the FW content in the BG. So despite the more favorable changes of the FW transport pathways in the ESS, the FW flux through the southern BG periphery did not vary significantly between 2003- 2008 and even slightly decreased in 2008 (Fig. 9). Thus, particles released in the Chukchi Sea have a somewhat better potential to affect the BG FW content during the period when the BG was not as intense as in 2008.

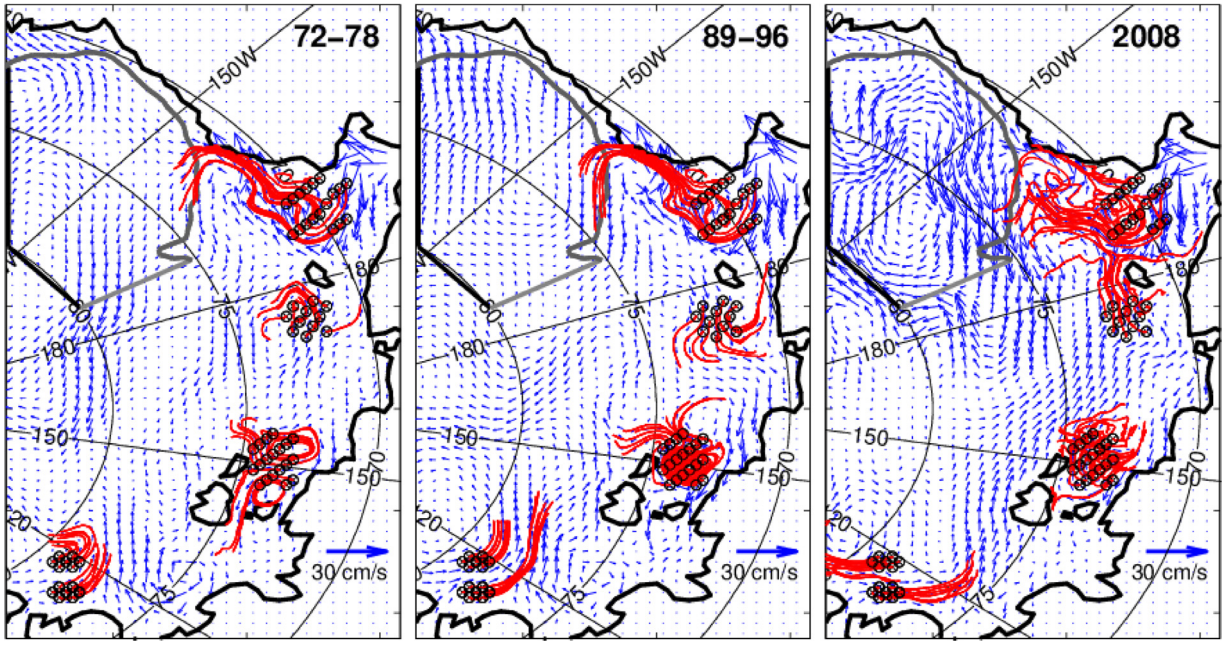

Fig. 11. The 6-month trajectory of the water parcels launched on July 1 at a 10m-depth in different years superimposed on the velocity fields averaged over respective periods. The BG integration area is shown.

4. Conclusions and discussion

This study addresses the analysis of the PSAO circulation in 2008, the first year of the 9-year period with the highest FW accumulation in the Beaufort Gyre. The 2008 circulation is compared with the circulations during three climatological periods corresponding to the positive (1972–1978, 1997–2006) and negative (1989–1996) phases of the AOO. In addition, a more detailed comparison is made with the PSAO states during the years of slow growth of the FW storage in the Beaufort Gyre (2003–2006).

The analysis has been performed by merging in situ hydrographic data, observations of the Bering Strait transport, and heat, salt and momentum fluxes with the dynamical constraints of a numerical model using a combination of two data assimilation systems. Validation of the results against independent SSH and velocity observations demonstrated a significantly better consistency with the data compared to the PIOMAS system, whose output was utilized as a first guess solution for subsequent 4dVar analysis.

The 4dVar reanalysis for the climatological periods of 1972–1978, 1989–1996, and 1997–2006, support and further quantify the concept of Proshutinsky and Johnson (1997), who suggested that the BG tends to accumulate FW during the anticyclonic AOO phase and release it during the negative phase. Our results also indicate that positive AOO phases are characterized by a larger inflow into the PSAO along the continental slope of the Laptev Sea, which brings the AW and tends to increase the total salt content in the Canadian Basin over a long term perspective. However, it is necessary to note that this result is obtained only for two particular periods of the positive AOO index and requires additional analysis for the last decade (2008–2017). There are also many other factors controlling the total FW content in the PSAO region, including the FW flow through the other open boundaries, ice drift and freshwater discharge which should be taken into account for a more accurate analysis of the FW content in the region.

In addition, we have found indications of FW accumulation in the East Siberian Sea during the cyclonic AOO phase (1989–1996) compared to the positive AOO phases (1972–1978, 1997–2006). This process has a prominent SSH signature in the form of a 15–20 cm high dome emerging in the western ESS (central panel in Fig. 4). Quantitative estimates show an increase of FW content in the ESS by 10% (500 km^3) during the negative AOO phases. The result is in quantitative agreement with the observational estimates of Dmitrenko et al. (2008b) who studied long-term variations of the FW content on the eastern Siberian shelf. However, our results for 2008 do not support this tendency. Possible reasons are due to the abnormally high discharge of the Siberian rivers (e.g. Charkin et al., 2011) and the drastic decrease of ice cover during 2007 and 2008 which may significantly impact the FW content in the shallow Siberian Shelf.

Of particular interest is the tendency of the Eurasian shelf water to follow the pathway through the Long Strait separating the Wrangel Island from the continent (low panels in Fig. 3). This tendency appears to be more visible during the cyclonic AOO phase, when even water parcels released northwest of the Wrangel Island are eventually found in the Long Strait. This circulation feature seems to support a remarkable persistence of the heavy ice conditions in the Long Strait during the relatively warm and humid summers which usually occur at the negative phase of the AOO index (Dunlap, 1996).

Analysis of the circulations during the positive and negative AOO phases indicates a larger SSH depression at the northern Chukchi Sea during the positive AOO phases suggesting a certain intensification of the Bering Strait throughflow during the positive AOO, but limited observational time span does not allow for a confident verification of this result.

The major focus of our study was the analysis of circulation features during the summer-fall season of the International Polar Year (2008) and the comparison of the 2008 circulation to circulations during previous years (2003–2006). The 2008 period was elected not only due to the unprecedented abundance of data, but also because it followed the year of a great ice melt anomaly (2007), which supplied the PSAO with an additional 1500 km^3 of fresh water and was the first year of a relatively long period of extremely high levels of FW accumulation in the BG. Analysis of the circulation and FW content in BG during 2003–2006, and 2008 indicate:

a) A reversal of the total transport in the AW inflow region of −2.9 Sv in July-August which later relaxed to an eastward transport of 0.8–1 Sv. The reversal of the along-slope current is confirmed by independent observations from NABOS moorings. Certain indications of the reversal are also found in the PIOMAS non-assimilative run.
b) Formation of a prominent SSH trough extending from the eastern Laptev Sea to the Bering Strait. A similar and even stronger structure was obtained in the PIOMAS solution and is indirectly evidenced by two NABOS moorings located on the continental slope of the Laptev Sea. The strengthening of the depression between 2003 and 2008 can also be traced in the CPOM-DOT monthly maps of Armitage et al. (2017). This feature amplified the BG and formed a 0.1 m/s strong current at the northern periphery of the Eurasian shelf.
c) The above mentioned SSH depression intensified the eastward flow north of the Wrangel Island and shortened the pathway of the fresh Siberian waters to the Bering Strait meridian, where they are engaged in mixing with the Pacific Water and in the circulation within the southern periphery of the BG. In addition, the SSH depression in the Chukchi Sea tends to increase the large-scale sea level difference between the Bering Sea and the Arctic Ocean, contributing to the 25% increase in the Bering Strait transport documented by Woodgate et al. (2010; 2012). The 2008 SSH depression also agrees with the analysis of the force balance in the Bering Strait, revealing an increased role of the pressure head between the Bering Sea and Arctic Ocean during 2007–2011 (Woodgate et al., 2012).
d) A significant increase of the FW content in the Beaufort Gyre from 16,700 km^3 in 2003 to 21,500 km^3 in 2008. The FW accumulation agrees well with the estimates made from in situ hydrographic observations obtained in the BGEP by Proshutinsky et al. (2009). The analysis of the FW transports across the BG boundaries indicate that FW accumulation in 2004–2008 was mainly caused by the anomalous inflow through the eastern section that changed from −0.1 Sv in the beginning of 2003 to 0.8 Sv inflow in 2008. The exact factors responsible for this FW inflow cannot be identified here, because our domain does not include the large part of the Arctic Ocean. However, the revealed FW inflow qualitatively agrees with the observational evidence of Lique et al. (2011) who diagnosed significant FW anomalies off of the Greenland coast and the hypotheses of A. Proshutinsky et al. (2015) explaining the extended positive AOO by the FW discharge from Greenland.
e) Weak interannual variability of the flow through the southern section suggests that changes of the FW pathways from the ESS as well as a certain increase of the Bering Strait transport provides only a minor contribution to the emergence of the FW anomaly in the Beaufort Gyre in 2008. Furthermore, the Lagrangian analysis and the above mentioned reduction of the FW flux through the southern section in 2008 suggests that the FW transport from the ES and Chukchi Seas into BG in 2008 was less than in 2003–2005.

Validation of the results by comparison with independent data indicates a significant improvement of the PIOMAS solution using

4dVar analysis. There are however, several limitations. First, is the absence of the explicit ice dynamics in the 4dVar system, which is simulated by the background ice-ocean fluxes from PIOMAS. This shortcoming does not allow explicit 4dVar analysis of the solid FW content in the Arctic Ocean. Such analysis can be done however, by a separate study of the PIOMAS DA output. Second, the utilized 4dVar system has an insufficient horizontal resolution to resolve any complicated processes in narrow straights, especially in the Bering Strait.

In view of the above, our analysis should be treated as preliminary, as it is limited by assimilating observations only in the PSAO region and by the two-stage assimilation system involving a state-of-the-art ice-ocean model equipped with a simple data assimilation scheme based on nudging, and an ocean-only model with an advanced 4dvar scheme. A more extensive study involving a synthesis of the entire IPY dataset with dynamic and thermodynamic constraints of a state-of-the-art ice-ocean model configured for the entire Arctic Ocean is necessary for further understanding the complex processes controlling the Arctic Ocean circulation. Our experience shows that getting access to new data and their preprocessing requires significant time and effort. It is therefore important to make all observations available for complex 4dVar analysis immediately after the field campaigns. This will allow for the operational tracking and monitoring of rapid changes occurring in the Arctic Ocean within the last decades.

Acknowledgments

This study was supported by the University of Hawaii, the International Arctic Research Center, NSF grants 1107925, 1203740, ARC-1107327, PLR-1416920 and PLR-1602985. The research was also supported by the Russian Government (grant no. 14, Z50.31.0012/03/19.2014). Max Yaremchuk and Gleb Panteleev were also supported by the ONR core project "Arctic data assimilation". The authors are indebted to Drs. I. Polyakov, T. Kikuchi, I. Semiletov for providing CTD meter and current data. The authors are also grateful to Dr. M. Tsamados and two anonymous reviewers whose recommendations helped to improve the manuscript.

References

Aksenov, Y., et al., 2016. Arctic pathways of Pacific Water: Arctic Ocean model intercomparison experiments. J. Geophys. Res. Oceans 121, 27–59. doi:10.1002/2015JC011299.

Armitage, T.W.K., Bacon, S., Ridout, A.L., Thomas, S.F., Aksenov, Y., Wingham, D.J., 2016. Arctic sea surface height variability and change from satellite radar altimetry and GRACE, 2003–2014. J. Geophys. Res. Oceans 121, 4303–4322. doi:10.1002/ 2015JC01157.

Armitage, T. W. K., Bacon, S., Ridout, A. L., Petty, A. A., Wolbach, S., Tsamados, M.: Arctic Ocean geostrophic circulation 2003-2014, The Cryosphere Discuss., doi:http://dx.doi.org/10.5194/tc-2017-22, in review, 2017.

Beszczynska-Moller, A., Fahrbach, E., Schauer, U., Hansen, e., 2012. Variability of Atlantic water temperature and transport at the entrance to the Arctic Ocean, 1997-2010. ICES J. Marine. Sci. 1–12. doi:10.1093/icesjms/fss056, Oxford University Press.

Bryan, K., 1969. A numerical method for the study of the circulation of the world oceans, Comput. Physics 4, 347–376.

Carmack et al., (2015) Toward Quantifying the increased role of oceanic heat in sea ice loss in the new Arctic BAMS, 2079–2106, http://dx.doi.org/10.1175/BAMS-D-13-00177.1.

Charkin, A.N., Dudarev, O.V., Semiletov, I.P., kruhmalev, A.V., Vonk, J.E., Sanchez-Garsia, L., Karlsson, E., Gustafsson, O., 2011. Seasonal and interannual variability of sedimentation and organic matter distribution in the Buor–Khaya Gulf: the primary recipient of input from Lena River and coastal erosion in the southeast Laptev Sea. Biogeosciences 8, 2581–2594 www.biogeosciences.net/8/2581/2011/ doi:10.5194/bg-8-2581-2011.

Cox, M.D., 1984. A Primitive equation, Three-Dimensional Model of the Oceans. Princeton University, Princeton, N. J. *GFDL Ocean Group Tech. Rep. No. 1*, Geophys. Fluid Dynamics Lab./NOAA.

De Steur, L., Steele, M., Hansen, E., Morison, J., Polyakov, I., Olsen, S.M., Melling, H., McLaughlin, F.A., Kwok, R., 2013. A freshwater anomaly passing through the Lincoln Sea in the Arctic Ocean, J. Geophys. Res. 118, 4699–4715 10.1002jgrc.20341.

Dmitrenko, I.A., Polyakov, I.V., Kirillov, S.A., Timokhov, L.A., Frolov, I.E., Sokolov, V.T., Simmons, H.L., Ivanov, V.V., Walsh, D., 2008. Toward a warmer Arctic Ocean: Spreading of the early 21st century Atlantic Water warm anomaly along the Eurasian Basin margins. J. Geophys. Res. 113, C05023. doi:10.1029/2007JC004158.

Dmitrenko, I.A., Kirillov, S.A., Tremblay, L.B., 2008. The long-term and interannual variability of summer fresh water storage over the eastern Siberian shelf: Implication for climatic change. J. Geophys. 113, C03007. doi:10.1029/2007JC004304.

Donlon, C.J., Martin, M., Stark, J.D., Roberts-Jones, J., Fiedler, E., Wimmer, W., 2012. The operational sea surface temperature and sea ice analysis (OSTIA) system, Remote Sens. Environ. 116, 140–158.

Dunlap, W.V., 1996. Transit passage in the Russian Arctic Straits. Maritime Briefing Series 1 (7) 70pp. ISBN 1-897643-21-7.

Francis, O.P., Panteleev, G.G., Atkinson, D.E., 2011. Ocean wave conditions in the Chukchi Sea from satellite and in situ observations. Geophys. Res. Lett. 38, L24610. doi:10.1029/2011GL049839.

Gent, P.R., McWilliams, J.C., 1990. Isopycnal mixing in ocean circulation models. J. Phys. Oceanogr. 20, 150–155.

Holloway, F.Dupont, Golubeva, E., Hakkinen, S., Hunke, E., Jin, M., Karcher, M., Kauker, F., Maltrud, M., Morales Maqueda, M.A., Maslowski, W., Platov, G., Stark, D., Steele, M., Suzuki, T., Wang, J., Zhang, J., 2007. Water properties and circulation in Arctic Ocean models. JGR 112, C04S03. doi:10.1029/2006JC003642.

IPCC, 2013. Climate Change 2013: The Physical Science Basis. In: Stocker, T.F., Qin, D., Plattner, G.-K., Tignor, M., Allen, S.K., Boschung, J. (Eds.), Contribution of Working Group I to the Fifth Assessment Report of the Intergovernmental Panel On Climate Change. Cambridge University Press, Cambridge, United Kingdom and New York, NY, USA, p. 1535. doi:10.1017/CBO9781107415324.

Jones, E.P., Anderson, L.G., Swift, J.H., 1998. Distribution of Atlantic and Pacific waters in the upper Arctic Ocean: implications for circulation, Geophys. Res. Lett 25, 765–768.

Jones, E.P., Anderson, L.G., et al., 2008. Is the global conveyor belt threatened by arctic ocean fresh water outflow?. In: Dickson, R., et al. (Eds.) Arctic-Subarctic Ocean Fluxes. Defining the Role of Northern Seas in Climate. Springer, New York, pp. 385–404.

Kalnay, E., et al., 1996. The NCEP/NCAR 40-year reanalysis project. Bull. Amer. Meteorol. Soc. 77, 437–471.

Kawaguchi, Y., Usuke, Y., 2015. Fixed-point observation of mixed layer evolution in the seasonally ice-free chukchi sea: turbulent mixing due to gale winds and internal gravity waves. J. Phys. Oceanogr. 45, 836–852.

Krishfield, R., K. Doherty, D. Frye, T. Hammar, J. Kemp, D. Peters, A. Proshutinsky, J. Toole, and K. von der Heydt, (2006) Design and operation of automated ice-tethered profilers for real-time seawater observations in the polar oceans, *WHOI-2006*-11, 79pp.

Kwok, R., Morison, J., 2011. Dynamic topography of the ice- covered Arctic Ocean from ICESat. Geophys. Res. Lett. 38, L02501. doi:10.1029/2010GL046063.

Large, W.G., and S. Pond, 1981: Open ocean momentum flux measurements in moderate to strong winds. J. Phys. Ocean., 11, 324–481

Large, W.G., McWilliams, J.C., Doney, S.C., 1994. Oceanic vertical mixing: A review and a model with a nonlocal boundary layer parameterization. Rev. Geophys. 32, 363–403.

Laxon, 2013. GryoSat-3 estimates of Arctic Sea ice thickness and volume, Geoph. Res. Lett (4) 723–737.

Le Dimet, F.-X., Talagrand, O., 1986. Variational algorithms for analysis and assimilation of meteorological observations: theoretical aspects. Tellus A 38 (2), 97–110.

Lindsay, R.W., Zhang, J., 2006. Assimilation of ice concentration in an ice-ocean model. J. Atmos. Oceanic Technol. 23, 742–749. doi:10.1175/JTECH1871.1.

Lique, C., Garric, G., Trguier, A.-M., Barnier, B., Ferry, N., Testut, C.-E., Girard-Ardhuin, F., 2011. Evolution of the Arctic Ocean salinity, 2007-2008: contrast between the Canadian and the Eurasian basins. J. Clim. 24 (3), 1705–1717.

Long, Z., Perrie, W., 2012. Air-sea interaction during an Arctic Storm. J.Geoph. Res. 20 V117, D15103.

Madec, G., Delecluse, P., Imbard, M., Levy, C., 1999. OPA8.1 Ocean General Circulation Model. Reference Manual. In: Note Du Pole Modelisation. Institute Pierre-Simon Laplace, IPSL, France, p. 91.

Manda, A., Hirose, N., Yanagi, T., 2005. Feasible method for the assimilation of satellite-derived SST with an ocean circulation model. JAOT 22 (6), 746–756. doi:10.1175/ JTECH1744.1.

Maslowski, W., Newton, B., Schlosser, P., Semtner, A., Martinson, D., 2000. Modeling recent climate variability in the Arctic Ocean. Geophys. Res. Lett. 27 (22), 3. doi:10.1029/1999GL011227, 743–3,746.

McIntosh, 1990. Oceanographic data interpolation: Objective analysis and splines. J. Geoph. Res 95, 13529–13541 C8.

McPhee, M., Proshutinsky, A., Morison, J.H., Steele, M., Alkire, M.B., 2009. Rapid change in freshwater content of the Arctic Ocean. Geophys. Res. Lett 36, L10602. doi:10.1029/2009GL037525.

McPhee, M. G., 2013. Intensification of Geostrophic Currents in the Canada Basin, Arctic Ocean. J. Climate 26 (10), 3130–3138.

Morison, J., Kwok, R., Peralta-Ferriz, C., Aikire, M., Rigor, I., Andersen, R., Steele, M., 2012. Changing Arctic Ocean freshwater pathways. Nature 481, 66–70. doi:10.1038/nature10705.

Nechaev, D., Panteleev, G., Yaremchuk, M., 2005. Reconstruction of the circulation in the limited region with open boundaries: circulation in the Tsushima Strait. Okeanologiya 45 (6), 805–828.

Panteleev, G., Nechaev, D., Ikeda, M., 2005. Reconstruction of summer Barents Sea circulation from climatological data. Atmosphere-Ocean 44 (2), 111–132.

Panteleev, G., Stabeno, P., Luchin, V.A., Nechaev, D., Ikeda, M., 2006. Summer transport estimates of the Kamchatka Current derived as a variational inverse of hydrophysical and surface drifter data. Geophys. Res. Lett. 33, L09609. doi:10.1029/2005GL024974.

Panteleev, G, Proshutinsky, A., Kulakov, M., Nechaev, D.A., Maslowski, W., 2007. Investigation of the summer Kara Sea circulation employing a variational data assimilation technique. J. Geoph. Res. 112, C04S15. doi:10.1029/2006JC003728.

Panteleev, G.G, M.Yaremchuk, D.Nechaev, 2008. Optimization of mooring observations in Northern Bering Sea. Dyn. Atmos. Oceans doi:10.1016/j.physletb.2003.10.071.

Panteleev, G., A.Proshutinsky, D.Nechaev, R.Woodgate, J.Zhang, 2010. Reconstruction and analysis of the Chukchi Sea circulation in 1990-1991. J. Geoph. Res 115 (C08023), 22. doi:10.1029/2009JC005453, 2010.

Panteleev, G., Yaremchuk, M., Stabeno, P., Luchin, V., Nechaev, D., Kikuchi, T., 2011. Dynamic topography of the Bering Sea. J. Geoph. Res 116. doi:10.1029/2010JC006354.

Panteleev, G., Yaremchuk, M., Francis, O., Kikuchi, T., 2013. Configuring High Frequency Radar observations in the Southern Chukchi Sea. Polar Science 7, 72–81.

Panteleev, G., Yaremchuk, M., Francis, O., Stabeno, P., Weingartner, T., Zhang, J., 2016. An inverse modeling study of circulation in the Eastern Bering Sea during 2007-2010. J. Geophys. Res. Oceans 121 3, 970-3,989, doi: 2015JC011287.

Pnyushkov, A., Polyakov, I., Ivanov, V., Aksenov, Ye., Coward, A., Janout, M., Rabe, B., 2015. Structure and variability of the boundary current in the Eurasian Basin of the Arctic Ocean. Deep-Sea Res.-I 101 (7), 80–97. doi:10.1016/j.dsr.2015.03.001.

Proshutinsky, A.Y., Johnson, M.A., 1997. Two circulation regimes of the wind-driven Arctic Ocean. J. Geophys. Res. 102. doi:10.1029/97JC00738, 12493–12514.

Proshutinsky, A., Bourke, R.H., McLaughlin, F.A., 2002. The role of the Beaufort Gyre in Arctic climate variability: Seasonal to decadal climate scales. Geophys. Res. Lett. 29 (23), 2100. doi:10.1029/ 2002GL015847.

Proshutinsky, A., Krishfield, R., Timmermans, M.-L., Toole, John, Carmack, E., Mclaughlin, F., Williams, W.J., Zimmermann, S., Itoh, M., Shimada, K., 2009. Beaufort Gyre reservoir: state and variability from observations. J. Geophys. Res. 114, C00A10. doi:10.1029/2008JC005104.

Proshutinsky, A., Dukhovskoy, D., Timmermans, M.-L., Krishfield, R., Bamber, J.L., 2015. Arctic circulation regimes. Phil. Trans. Roy. Soc. A 373, 20140160.

Qiao, F., Yeli, Yuan, Yongzeng, Yang, Quanan, Zheng, Changshui, Xia, Jian, Ma, 2004. Wave-induced mixing in the upper ocean: Distribution and application to a global ocean circulation model. Geophys. Res. Lett. 31, L11303. doi:10.1029/2004GL019824, 2004.

Rabe, B., Karcher, M., Schauer, U., Toole, J.M., Krishfield, R.A., Pisarevc, S., Kauker, F., Gerdes, R., Kikuchi, T., 2011. An assessment of Arctic Ocean freshwater content changes from the 1990 s to the 2006–2008 period. Deep Sea Res 58 (5), 173–185.

Reynolds, R.W., Rayner, N.A., Smith, T.M., Stokes, D.C., Wang, W., 2002. An improved in situ and satellite SST analysis for climate. J. Climate 15, 1609–1625.

Roach, AT, Aagaard, K, Peas7, CH, Salo, S.A., Weingartner, T, Pavlov, V, Kulakov, M, 1995. Direct measurements of transport and water properties through the Bering Strait. J Geophys Res. 100, 18443–18457.

Schlax, M.G, Chelton, D.B., 1994. Detecting aliased tidal errors in altimeter height data. J. Geoph. Res. 99 (C12), 24 761-24,775.

Schlax, M.G, Chelton, D.B., 1994. Detection aliased tidal errors in altimeter height measurements. J. Geoph. Res. 99 (C6), 12 603-12,612.

(Ed) Semtner Jr., A.J., 1986. Finite-difference formulation of a world ocean model. In: O'Brien, J., Riedel, D. (Eds.), Proc. NATO Advanced Physical Oceanographic Numerical Modeling, pp. 187–202. (Ed).

Smith, R.D., Dukowicz, J.K., Malone, R.C., 1992. Parallel Ocean General Circulation Modeling. Physica D 60, 38–61.

Stark, J.D., Donlon, C.J., Martin, M.J., McCulloch, M.E., 2007. OSTIA: An operational high resolution real-time global sea surface temperature analysis system, paper presented at *Oceans 2007: Marine Challenges: Coastline to Deep Sea*. IEEE/Oceanic. Eng. Soc. Aberdeen, Scotland, 18-21 June.

Steiner, N., Holloway, G., Gerdes, R., Haakkinen, S., Holland, D., Karcher, M., Kauker, F., Maslowski, W., Proshutinsky, A., Steele, M., Zhang, J., 2004. Comparing modeled streamfunction, heat and freshwater content in the Arctic Ocean. Ocean Modell. 6, 265–284.

Stroh, J.N., Panteleev, G., Kirillov, S., Makhotin, M., Shakhova, N., 2015. Sea surface temperature and salinity product comparison against externa; in situ data in the Arctic Ocean. J. Geophys. Res. Oceans 120. doi:10.1002/2015JC011005, 7,223-7,236.

Wang, J., Mizobata, K., BAI, X., HU, H., Jin, M., Yu, Y., Ikeda, M., Johnson, W., Perie, W., FUJISAKI, A., 2014. A modeling study of coastal circulation and landfast ice in the nearshore Beaufort and Chukchi Seas using CIOM. J. Geophys. Res. 28, 3285–3312. doi:10.1002/2013JC009258.

Wang, Q., Coauthors, 2016. An assessment of the Arctic Ocean in a suite of interannual CORE-II simulations. Part I: Sea ice and solid freshwater. Part II: Sea ice and solid freshwater. Ocean Modell. 99, 86–132. doi:10.1016/j.ocemod.2015.12.008.

Weingartner, T., Danielson, S., Sasaki, Y., Pavlov, V., Kulakov, M., 1999. The Siberian Coastal Current: A wind- and buoyancy-forced Arctic coastal current. J. Geoph.Res. 104 (C12), 29697–29713. doi:10.1029/1999JC90016.

Williams, T.D, Bennetts, L.G., Squire, V.A., Dumont, D., Bertino, L., 2013. Wave–ice interactions in the marginal ice zone. Part 1: Theoretical foundations. Ocean Modell. 71, 81–91.

Williams, T.D., Bennetts, L.G., Squire, V.A., Dumont, D., Bertino, L., 2013. Wave-ice interactions in the marginal ice zone. Part 2: numerical implementation and sensitivity studies along 1D transects of the ocean surface. Ocean Modell. 71, 92–101.

Woodgate, R.A, Aagaard, K, Weingartner, T.J, 2005. Monthly temperature, salinity, and transport variability of the Bering Strait throughflow. Geophys Res Lett 32, L04601 87210.1029/ 2004GL021880.

Woodgate, R.A., Aagaard, K., Weingartner, T.J., 2006. Interannual changes in the Bering Strait fluxes of volume, heat and freshwater between 1991 and 2004. Geophys. Res. Lett. 33, L15609. doi:10.1029/2006GL026931.

Woodgate, RA, Aagaard, K, Weingartner, TJ, 2007. First steps in calibrating the Bering Strait throughflow: Preliminary study of how measurements at a proposed climate site (A3) compare to measurements within the two channels of the strait (A1 and A2), 20. University of Washington.

Woodgate, R.A., Weingartner, T.J., Lindsay, R.W., 2010. The 2007 Bering Strait Oceanic Heat Flux and anomalous Arctic Sea-ice Retreat. Geophys. Res. Lett. 37, L01602. doi:10.1029/2009GL041621.

Woodgate, R.A., Weingartner, T.J., Lindsay, R., 2012. Observed increases in Bering Strait oceanic fluxes from the Pacific to the Arctic from 2001 to 2011 and their impacts on the Arctic Ocean water column. Geophys. Res. Lett. 39 (24), 6. doi:10.1029/2012gl054092.

Woodgate, R.A., Stafford, K.M., Prahl, F.G., 2015. A synthesis of year-round interdisciplinary mooring measurements in the Bering Strait (1990–2014) and the RUSALCA years (2004–2011). Oceanography 28 (3), 46–67. doi:10.5670/oceanog.2015.57.

Yang, J., Comiso, J., Walsh, D., Krishfield, R., Honjo, S., 2004. Storm-driven mixing and potential impact on the Arctic Ocean. J. Geophys. Res. 109, C04008. doi:10.1029/ 2001JC001248.

Zhang H.S. (2009). The Report of 2008 Chinese Arctic Research Expedition (in Chinese). Beijing: China Ocean Press. 206p

Zhang, J., Rothrock, D.A., 2001. A thickness and enthalpy distribution sea ice model. J. Phys. Oceanogr. 31, 2986–3001.

Zhang, J., Rothrock, D.A., 2003. Modeling global sea ice with a thickness and enthalpy distribution model in generalized curvilinear coordinates. Mon. Weather Rev. 131 (5), 681–697.

Zhang, J., Rothrock, D.A., 2005. The effect of sea ice rheology in numerical investigations of climate. J. Geophys. Res. 110, C08014. doi:10.1029/2004JC002599.

Zhang, J., Lindsay, R., Schweiger, A., Steele, M., 2013. The impact of an intense summer cyclone on 2012 Arctic sea ice retreat. Geophys. Res. Lett. 40, 720–726. doi:10.1002/grl.50190.

Zhang, J., Ashjian, C., Campbell, R., Spitz, Y.H., Steele, M., Hill, V., 2015. The influence of sea ice and snow cover and nutrient availability on the formation of massive under-ice phytoplankton blooms in the Chukchi Sea. Deep-Sea Res. II 118, 122–135. doi:10.1016/j.dsr2.2015.02.008.

Zhang, J, Steele, M, Runciman, K, Dewey, S, Morison, J, Lee, C, Rainville, L, Cole, S, Krishfield, R, Timmermans, M.-L, Toole, J, 2016. The Beaufort Gyre intensification and stabilization: A model-observation synthesis. J. Geophys. Res. Oceans 121. doi:10.1002/2016JC01219.